https://doi.org/10.5194/egusphere-2026-1398
Preprint. Discussion started: 8 April 2026

Beneath the tide: Sediment-controlled groundwater and salinity stratification across an estuarine wetland transect

Christopher J. Owers[1], Rachel McGivern[1], Warren Brown[2], and Gabriel C. Rau[1]

[1]Earth Sciences, School of Science, The University of Newcastle, NSW, Australia
[2]Central Coast Council, NSW State Government, NSW, Australia

Correspondence: Christopher J. Owers (chris.owers@newcastle.edu.au)

Abstract. Coastal vegetated wetlands occur at the interface between marine and terrestrial hydrological processes, yet the subsurface controls governing salinity persistence and vegetation zonation remain poorly constrained, particularly in settings where wave energy is suppressed, such as barrier estuaries. We investigate seawater–groundwater interactions along a transect spanning mangrove, saltmarsh, supratidal, and terrestrial vegetation zones using electrical resistivity tomography (ERT), water-level and salinity monitoring, and sediment analysis. Results reveal a pronounced lateral and vertical salinity structure characterised by a shallow saline wedge extending inland within fine-grained intertidal sediments, while deeper groundwater remains comparatively fresh. Vegetation zonation closely mirrors this subsurface composition: mangrove and saltmarsh communities are associated with persistent shallow salinity in low-permeability silt–clay substrates, whereas supratidal and terrestrial vegetation occurs where sandier sediments and less saline water dominate. Although rainfall and tidal forcing dynamically influence shallow groundwater, salinity variability attenuates rapidly with depth, indicating limited vertical connectivity and sediment-controlled hydraulic anisotropy. The persistence of fresh groundwater beneath saline shallow sediments departs from the classical homogeneous, density-driven coastal aquifer model. Instead, the system reflects a hydraulically stratified composition in which fine-sediment accretion promotes vertical permeability contrasts and shallow saline retention, while deeper freshwater-dominated zones (indicated by low bulk electrical conductivity, potentially reflecting terrestrially recharged groundwater) extend towards the estuary. This vertically differentiated configuration influences vegetation distribution and contributes to carbon-rich intertidal sediment accumulation. We propose a refined conceptual model for microtidal, wave-dominated barrier estuaries with similar sedimentary infilling histories, emphasising sediment-controlled hydraulic anisotropy over density-driven stratification.

https://doi.org/10.5194/egusphere-2026-1398
Preprint. Discussion started: 8 April 2026

1 Introduction

Coastal vegetated wetlands, such as mangrove and saltmarsh, are highly dynamic environments that occur at the interface between land and sea (Saenger, 2002; Townend et al., 2011). They are typically positioned along low-energy coastlines within protected embayments and estuaries, where wave action is limited and sediment deposition can occur (Thom, 1967; Boyd et al., 1992; Allen, 2000). These environments provide a wide range of important ecosystem services, including shoreline protection from erosion and storm surges, support for high levels of biodiversity, and long-term carbon storage supporting climate mitigation (Ewel et al., 1998; Barbier et al., 2011; Lee et al., 2014; Macreadie et al., 2021). Despite their ecological and societal importance, coastal wetlands are particularly sensitive to climate-related pressures such as sea-level rise, altered rainfall regimes, and increasing temperatures (Lovelock et al., 2015; Friess et al., 2019; Saintilan et al., 2023a). At the same time, these ecosystems display a notable degree of resilience, often responding to environmental change through vertical and lateral changes in vegetation distribution (Rogers et al., 2014; Saintilan et al., 2023b; Lal et al., 2024).

Coastal wetlands are typically divided into subtidal, intertidal, and supratidal zones, each defined by observed vegetation communities, tidal inundation regimes, and their tolerance for saline conditions (Adame et al., 2024). The subtidal zone, continually submerged, primarily hosts seagrasses, while the intertidal zone, which includes mangroves and saltmarsh, experiences periodic tidal inundation, supporting varied plant species adapted to saline conditions (Pennings et al., 2005; Kumbier et al., 2021a). Extensive research has focused on these intertidal environments, providing a strong understanding of the ecological processes governing mangrove and saltmarsh systems. In contrast, considerably less is known about the environments that occur landward of the intertidal zone, particularly the supratidal and adjacent terrestrial vegetated areas (Kelleway et al., in review). The supratidal zone, located higher in the tidal frame above the level of mean high water for spring tides, remains largely free from regular tidal inundation, experiencing inundation as a result of storm surge and metrological events (Kelleway et al., 2025). In Australia, this zone is often colonised with vegetation such as *Casuarina* and *Melaleuca* species adapted to occasional saltwater exposure (Tran et al., 2015; Adame et al., 2024; Kelleway et al., 2021a, 2025).

Surface elevation within coastal wetlands is critical to resilience against sea level rise, as vegetation roots in mangroves and saltmarsh stabilise sediment and facilitate organic matter accumulation, enabling gradual elevation increases (Cahoon et al., 2006; Lovelock et al., 2015; Woodroffe et al., 2016; Rogers et al., 2019). This process counters inundation risks and maintains ecosystem resilience in the face of changing sea levels (Saintilan et al., 2023b). Rising sea levels are expected to progressively alter the tidal frame in which wetland ecosystems occur, potentially reshaping the distribution and composition of vegetation communities. A substantial body of work has demonstrated strong relationships between ground surface elevation, tidal inundation regimes, and vegetation patterns, showing that even small changes in elevation can result in major lateral changes in distribution over time (Rogers et al., 2022; Saintilan et al., 2023a).

Groundwater dynamics are a crucial but often overlooked component of coastal wetland ecosystems (Sadat-Noori et al., 2025). The groundwater dynamics of coastal wetlands are influenced by tidal fluctuations and the freshwater-saltwater interface, where density differences between fresh and saline water create a distinct subsurface lens of freshwater (Palombi et al., 2026). This interface supports vegetation by providing an accessible freshwater source, crucial in areas otherwise dominated

https://doi.org/10.5194/egusphere-2026-1398
Preprint. Discussion started: 8 April 2026

by brackish or saline waters (Jiao and Post, 2019b). Tidal influences shape coastal wetland ecosystems by modulating salinity gradients, inundation frequency, and nutrient availability, which in turn affect plant community composition and zonation patterns (Glamore et al., 2016).

The contribution of groundwater to coastal wetland functioning has hitherto been overlooked (Guimond, 2025). Coastal groundwater systems, particularly in tidal wetland areas, are vulnerable to climate change impacts, including sea level rise and altered precipitation patterns (Sadat-Noori et al., 2025). The equilibrium between freshwater and saltwater is influenced by factors such as precipitation, temperature, and sea levels, where changes in these conditions can influence recharge (the process by which groundwater is replenished, primarily through precipitation), temperature, and chemical composition of groundwater (e.g., Zhang et al., 2018). Sea level rise increases the likelihood for saltwater intrusion into coastal aquifers, posing risks to freshwater availability for vegetation and compromising wetland resilience (Krauss et al., 2010; Sadat-Noori et al., 2025). Shifts in vegetation distribution and condition within coastal wetlands occur as a response to these changes, and the capacity of vegetated wetland communities adapting through sediment accumulation and surface elevation maintenance, may be critical in determining how effectively they can cope with these ongoing environmental pressures (Saintilan et al., 2019). Given the uncertainty surrounding the function of groundwater in coastal wetland areas, it is difficult to quantify the magnitude of the impacts and consequences of climate change. Long-term monitoring data for coastal groundwater is limited, making it challenging to identify patterns of vegetation response, and track changes over time (Lorrain-Soligon et al., 2023; Sadat-Noori et al., 2025).

This study addresses critical knowledge gaps in surface–groundwater interactions and ecosystem function within vegetated coastal wetlands, particularly the hydrological and salinity dynamics of supratidal forests. Despite their increasing relevance for coastal carbon storage and climate resilience, these transitional environments remain poorly constrained. The primary aim is to investigate hydrological connectivity, saltwater-freshwater mixing processes, and edaphic conditions on vegetation distribution across a tidal-to-terrestrial gradient. By integrating electrical resistivity tomography, hydrological monitoring, and sedimentological analysis across mangrove, saltmarsh, supratidal forest, and terrestrial vegetation zones, we examine how coupled above- and below-ground processes influence coastal ecosystem composition. Specifically, the objectives are to: (a) establish a long-term hydrological and salinity monitoring framework across the vegetation gradient; (b) characterise surface-groundwater interactions and sediment composition; (c) identify spatial and temporal dynamics of seawater-freshwater interfaces; and (d) conceptualise a hydrogeological model integrating subsurface structure with vegetation zonation. We propose a refined conceptual model in which sedimentary composition governs vertical groundwater stratification in low-energy barrier estuaries, extending beyond the scope of the classical freshwater-lens paradigm to provide a mechanistic basis for predicting ecosystem response to sea-level rise.

https://doi.org/10.5194/egusphere-2026-1398
Preprint. Discussion started: 8 April 2026

2 Methodology

2.1 Study Setting

This research was conducted at Kylie Close Wetland in Bensville on the Central Coast of New South Wales, Australia (Figure 1). The Central Coast has a temperate climate with warm, humid summers and mild winters, with annual rainfall ranging from 1200-1600 mm (Beck et al., 2023; DCCEEW). Bensville wetland is located within Empire Bay of the Brisbane Waters Estuary, a wave dominated barrier estuary, with a catchment area of 170 km^2 and estuary area of approximately 27 km^2 (Roy et al., 2001). The Brisbane Water Estuary, around Empire Bay, is characterised by sandy barrier formations shaped by longshore drift and wave action, with predominant quartzose sands typical of Australia's southeast coastline (Harvey and Caton, 2003). The site is underlain by unconsolidated estuarine and alluvial sediments of variable grain size, overlying weathered Hawkesbury Sandstone, which exerts a strong control on groundwater storage and flow pathways. Tides in Brisbane Water estuary are semi-diurnal, and propagate through the estuary entrance at Broken Bay, with a tidal range of 1.028 m (measured at Koolewong (ID 2124301) between 2001-2020) (MHL).

The study examines Bensville vegetation communities along an ecological gradient from intertidal to supratidal and terrestrial zones (Figure 1). The Mangrove (MG) zone, dominated by *Avicennia marina* with some *Aegiceras corniculatum* present, consists of small to medium-sized trees (3–10 m) that occupy the lowest position in the tidal frame (at or near mean sea level (MSL)). The mangrove saltmarsh Ecotone (ET) reflects a transitional area with overlapping mangrove and saltmarsh species (Saintilan, 2009). Further landward, the Saltmarsh (SM) zone, dominated by *Sarcocornia quinqueflora*, extends toward the Highest Astronomical Tide (HAT), typical of many settings in southeast Australia (Owers et al., 2016b).

Beyond the intertidal zone, *Casuarina Glauca* and *Melaluca quinquenervia* colonise the supratidal zone. For this study, the supratidal forest was categorised as Lower Supratidal Forest (LSTF) and Upper Supratidal Forest (USTF) based on vegetation morphology and Electrical Resistivity Tomography (ERT) measurements, highlighted further in section 2.2, and could be considered similar to existing literature differentiating fringe and interior supratidal forest (Kelleway et al., 2025). The LSTF was dominated by *Casuarina glauca*, reaching up to 20 m in height, and *Melaleuca quinquenervia* alongside *Juncus kraussii*, a perennial rush forming dense clumps up to 1.5 m in height (Kelleway et al., 2021b; Atlas of Living, 2007; Owers et al., 2016a). The USTF area consists of *Melaleuca quinquenervia*, medium-sized tree reaching 10–20 m (Fernandez Winzer et al., 2018), and Sword-sedge (*Gahnia spp.*), a robust grass-like plant up to 1 m tall, adapted to edaphic conditions of the upper supratidal zone (Victoria, 2020). The terrestrial area, beyond tidal influence of surface water, had a medium-dense understory of *Pteridium esculentum*, a common fern, with large trees 20-30 m in height dominated by the native Swamp Mahogany (*Eucalyptus robusta*).

Previously agricultural land, the area has been under local council management since the 1960s, with Landcare programs initiated in the 2010s to control invasive species, particularly asparagus fern. This geological and ecological setting makes Bensville wetland well suited for investigating interactions between tidal forcing, groundwater dynamics, salinity distributions, and vegetation zonation across coastal wetland–terrestrial transitions.

https://doi.org/10.5194/egusphere-2026-1398
Preprint. Discussion started: 8 April 2026

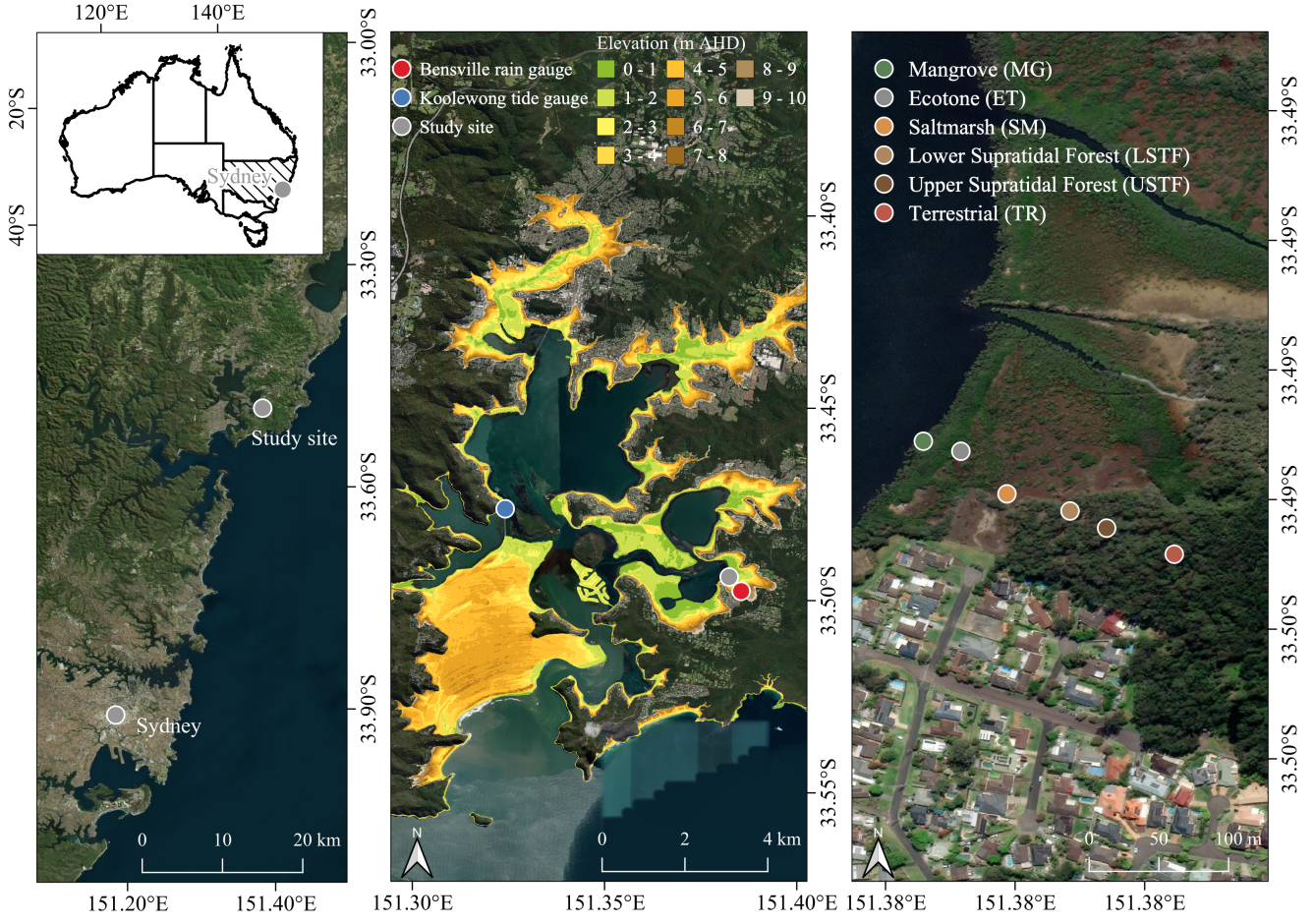

Figure 1. Location of the Bensville wetland study site with the Brisbane Water Estuary of New South Wales, Australia. Figure shows location of nearest rain and tide gauges to study site, overlain on Digital Elevation Model (DEM). Monitoring locations for each vegetation type are also presented. Source: DEM, 5 m seamless mosaic from Elvis Spatial Portal; Imagery, Bing World Imagery.

2.2 Electrical resistivity tomography

Monitoring locations for surface water and shallow groundwater instrumentation were selected using electrical resistivity tomography (ERT) to characterise subsurface bulk resistivity along transects oriented perpendicular to the seaward boundary of the site (Figure 1). ERT was employed as a non-invasive screening tool to identify subsurface salinity gradients and stratigraphic contrasts relevant to groundwater–surface water interactions, thereby informing the placement of monitoring infrastructure.

ERT surveys were conducted using an *ABEM Terrameter LS system* (Guideline Geo AB, Sweden) equipped with 64 channels. Three transects were separately acquired to support the selection of water monitoring locations. All surveys were conducted using a gradient array configuration, in which current was injected through distant electrode pairs while voltages were measured

https://doi.org/10.5194/egusphere-2026-1398
Preprint. Discussion started: 8 April 2026

across intermediate electrodes. This configuration enhances data redundancy and improves inversion robustness through the use of multiple electrode combinations.

The first transect (ERT-1), surveyed on 21 February 2024, targeted the lower supratidal forest to terrestrial zone (LSTF to TR), to establish baseline subsurface conditions. This transect employed a 2.5 m electrode spacing and covered approximately 147.5 m using 60 electrodes. A second transect (ERT-2) was surveyed on 12 June 2024 following a storm surge event to assess whether subsurface conditions relevant to monitoring site selection were consistent with those observed in February. This transect also used a 2.5 m electrode spacing and covered approximately 145 m using 59 electrodes. The third transect (ERT-3), surveyed on 5 September 2024, employed a wider 5 m electrode spacing and covered approximately 185 m using 38 electrodes. This transect extended from the mangrove saltmarsh ecotone (ET), to the lower supratidal forest (LSTF) to provide broader spatial context for delineating monitoring zones.

ERT data were screened to remove outliers (e.g., negative apparent resistivities) and inverted using *ResIPy* (Blanchy et al., 2020). Inversions targeted a root-mean-square (RMS) data misfit below 3%. Changes in elevation across the transect were not considered during the inversion. Inverted resistivity models were subsequently expressed as bulk electrical conductivity (EC_B) to facilitate comparison with groundwater and surface water electrical conductivity measurements (EC_W) collected during field monitoring. Individual inverted transects were spatially aligned and combined to provide a continuous representation of subsurface conductivity across the study area. Spatial patterns in EC_B, together with vegetation community composition, were used as criteria for selecting drilling and monitoring locations. These criteria ensured that monitoring infrastructure was positioned across representative hydrogeological and ecological zones spanning intertidal, supratidal, and terrestrial environments across the complex estuary-wetland vegetation gradient.

2.3 Monitoring of water levels, salinity and precipitation

Surface water levels were monitored using piezometres installed to depths of approximately 0.5 m below ground level at six locations along the coastal vegetation transect: Mangrove (MG), mangrove saltmarsh Ecotone (MSE), Saltmarsh (SM), Lower Supratidal Forest (LSTF), Upper Supratidal Forest (USTF), and Terrestrial (TR) zones (Figure 1). piezometres were installed using a post driver and consisted of laser-slotted PVC pipes, sealed at the base, with PVC driving points and wrapped in geotextile to permit hydraulic connectivity while minimising sediment ingress. Groundwater piezometres were installed using a hand auger (Royal Eijkelkamp, The Netherlands) to depths between 3 and 5 m below ground level at the LSTF, USTF, and TR zones (Figure 2). Sediments were retrieved during drilling using a bailer and logged to develop simplified lithological profiles. Each piezometre was completed with a 50 mm diameter PVC casing incorporating a 0.5 m screened interval wrapped in geotextile. The annulus surrounding the screened section was backfilled with clean river sand, and the upper section was sealed using bentonite pellets to prevent vertical leakage and surface water ingress. Each surface water monitoring location was measured using real-time kinematic global navigation satellite system (RTK-GNSS) surveys conducted with an EMLID Reach RS4 receiver. Under open-sky conditions, reported horizontal and vertical accuracies were approximately 5 mm and 12 mm, respectively; accuracy decreased beneath dense canopy cover however all recorded surface water monitoring locations were measured as fixed RTK-GNSS points. All elevations were reported in the Australian Height Datum (AHD), where 0 m

https://doi.org/10.5194/egusphere-2026-1398
Preprint. Discussion started: 8 April 2026

AHD approximates MSL across Australia determined from tidal gauges around the Australian coastline. All data was recorded in Geocentric Datum of Australia (GDA2020).

Water levels were recorded using pressure transducers mounted within each surface water and groundwater piezometre. Sensors consisted of a combination of HOBO (Onset Computer Corporation, USA) and Levelogger (Solinst, Canada) instruments and logged absolute pressure at 15- or 30-minute intervals, depending on deployment period and sensor type. Manual water-level measurements were collected during multiple field campaigns (14 March 2024, 6 June 2024, 5 September 2024, 6 February 2025, and 17 December 2025) to support sensor calibration and quality control. A barometric pressure sensor was installed on site to allow compensation of absolute pressure measurements (Rau et al., 2019).

Water electrical conductivity (EC_W) was monitored using *HOBO U24* capacitance loggers (Onset Computer Corporation, USA) installed at selected surface water and groundwater locations within the LSTF and USTF zones. Conductivity was recorded at 15- or 30-minute intervals and data were downloaded during site visits and stored in standardised date-time format. During post-processing, timestamps were corrected for *Daylight Saving Time*, and artefacts at the beginning and end of each deployment period were removed. Short periods affected by barometric sensor absence or malfunction were corrected using linear interpolation. All EC_W and bulk electrical conductivity (EC_B) values were reported in mS cm^{-1} to ensure consistency with ERT-derived conductivity estimates.

Hydraulic head was derived from absolute pressure transducer measurements by removing atmospheric pressure (i.e., barometric compensation) and converting water pressure to hydraulic head. Because pressure transducers were not individually surveyed to a common vertical datum, a site-specific offset was applied based on manual depth-to-water measurements. Continuous hydraulic head time series were calculated as

$$h(t) = h_{offset}(t_i) + \frac{p(t) - p_{atm}(t)}{\rho(t)\, g}, \tag{1}$$

where $p(t)$ is the recorded absolute pressure (Pa), $p_{atm}(t)$ is atmospheric pressure (Pa), $\rho(t)$ is fluid density (kg m^{-3}), g is gravitational acceleration (9.796 m s^{-2}), t denotes the discrete measurement times of the pressure transducer, and t_i denotes the discrete times at which manual depth-to-water measurements were obtained. The offset term $h_{offset}(t_i)$ anchors the pressure-derived head to the surveyed vertical datum and was calculated at each manual measurement time as

$$h_{offset}(t_i) = z_{loc} - h_{loc}^{dip}(t_i) - \frac{p(t_i) - p_{atm}(t_i)}{\rho(t_i)\, g}, \tag{2}$$

where z_{loc} is the surveyed elevation of the sensor reference point (m AHD) and $h_{loc}^{dip}(t_i)$ is the manually measured depth to water (m) at time t_i. Between manual measurements, h_{offset} was assumed constant (or linearly interpolated between successive manual measurements) and applied to the continuous pressure record to obtain a continuous hydraulic head time series (Rau et al., 2019).

Fluid density was calculated as a function of electrical conductivity and temperature using the *TEOS-10 Gibbs Seawater* formulation implemented in Python (McDougall and Barker, 2011). Electrical conductivity of estuary seawater was indepen-

https://doi.org/10.5194/egusphere-2026-1398
Preprint. Discussion started: 8 April 2026

dently measured at approx. 53 mS cm^{-1} and used as a reference for density estimates in tidally influenced surface waters. All time series were collated and resampled to 15-minute intervals using linear interpolation to enable consistent comparison across sensors prior to hydraulic head calculation.

Rainfall and tidal water-level data for the monitoring period (March 2024–December 2025) were obtained from the *Koolewong* tide gauge (Station ID 2124301) and the *Bensville* rain gauge (Station ID 561144), operated by the *NSW Government's Manly Hydraulics Laboratory* (Figure 1). These data were used to contextualise observed surface water and groundwater level variability. Data were converted from older to newer datum (e.g., GDA94 to GDA2020) where required. Long-term tidal planes were also obtained with values of 0.118 mAHD for mean sea level (MSL), -0.25 mAHD for lowest astronomical tide (LAT) and 0.78 mAHD for highest astronomical tide derived from data spanning 2001-2020.

Surface water depth time series were analysed to calculate inundation range, inundation frequency and inundation duration for each vegetation zone, following the approach of Kumbier et al. (2021b). This was undertaken to identify spatial and temporal dynamics of surface water in relation to seawater-freshwater interfaces. All analysis was completed using Python programming language and reported in m AHD using GDA2020.

2.4 Sediment collection and analysis of properties

To characterise sediment composition, sediment cores were collected in each vegetation zone near surface and groundwater piezometres. A total of six cores were collected; mangrove (MG), ecotone (ET), saltmarsh (SM), lower supratidal forest (LSTF), upper supratidal forest (USTF), terrestrial forest (TR). 1 m sediment cores were collected using a Russian peat corer, obtained in two 50 cm sections, photographed, and sub-sampled into 10 cm increments. Recovered samples were taken to the laboratory and kept at 4°C in a temperature-controlled facility until analysis. In the laboratory, each sub-sample was transferred onto a tray, carefully dissected to identify root matter, which were visually classified by size (fine, medium, large) and recorded as abundant or sparse (Conroy et al., 2025). Presence of shell material was also recorded.

Sediment sample wet weight was recorded, followed by oven-drying at 105°C for 24 hours to determine dry weight, and calculate dry bulk density ($g\,cm^{-3}$) and moisture content (%). Organic matter content was determined by loss-on-ignition (LOI) at 550°C for 4 hours (Heiri et al., 2001). Percent organic carbon (% C) was estimated using previously established relationships between % C and LOI for coastal vegetated wetlands of southeast Australia (Owers et al., 2016a; Kelleway et al., 2021a, 2025).

Grain size for each sediment sample was determined using a *Malvern Mastersizer 2000*, which uses laser diffraction to determine particle size distribution. The laser scattering data, processed using Mie theory (Wriedt, 2012), yielded particle sizes from sub-micron to millimetre scale. The grain size classifications are as follows: clay is defined as particles smaller than 2 μm, silt ranges from 2 to 20 μm, and sand ranges from 20 to 2000 μm. Results were presented as grain size distributions. If initial measurements varied, samples were re-measured, averaging 3–6 distributions to calculate clay, silt, and sand percentages (Malone and Searle, 2021). Sediment grain size was described as sand, sandy loam, loam, loamy sand, and silt loam.

The relationship between grain size distribution and hydraulic conductivity (K) is well established in hydrogeology, with empirical equations such as the Hazen formula ($K = C \times d_{10}^2$, where $C \approx 1.0$ for natural sands at 10°C; Hazen 1892) for

https://doi.org/10.5194/egusphere-2026-1398
Preprint. Discussion started: 8 April 2026

sand-dominated sediments and the Kozeny-Carman equation (accounting for porosity and specific surface area; Kozeny 1927; Carman 1997; Rosas et al. 2013) for mixed and fine-grained materials providing order-of-magnitude estimates of K from textural data. While such estimates offer indicative permeability ranges for different depositional environments, precise quantification of absolute K values and anisotropy ratios (K_v/K_h) would require laboratory testing of intact cores or field hydraulic tests (e.g., slug tests, permeameter measurements), which were not conducted in this study (Vienken and Dietrich, 2014).

Sample pore water salinity was measured by taking a 20 g sub-sample and combining with 100 mL deionised water, stirred, and allowed to settle for EC_W measurement using a conductivity meter. Pore water salinity ($S_{\text{pore water}}$) was calculated from the measured solution salinity (S_{solution}) and water content, reflecting original pore water salt concentrations. First, the volume of water originally present in the sediment ($V_{\text{water in sediment}}$) was determined using the water content percentage and the wet weight of the sediment

$$V_{\text{water in sediment}} = \frac{\text{Water Content} \times \text{Wet Weight}}{100}.$$

Given that the density of water is approximately 1 g/cm^3, the mass of water in grams equals the volume in millilitres (mL). The pore water salinity was then calculated by adjusting the measured solution salinity based on the ratio of the total water volume to the original pore water volume

$$S_{\text{pore water}} = S_{\text{solution}} \times \frac{V_{\text{deionised water}} + V_{\text{water in sediment}}}{V_{\text{water in sediment}}},$$

where $V_{\text{deionised water}}$ is the volume of deionised water added (100 mL). Descriptive salinity classes were then determined based on descriptions relative to seawater (50-55 mS cm^{-1}) (Bear et al., 1999; Custodio and Bruggeman, 1987).

3 Results

3.1 Site setup and shallow lithology

The long-term monitoring transect was established at Bensville to address key knowledge gaps in the understanding of surface–groundwater interactions across a complex coastal wetland vegetation gradient (Figure 2). Results from the ERT surveys, together with vegetation community composition, were used as criteria for selecting drilling and monitoring locations. Six piezometres were installed to measure surface water dynamics, with an additional three piezometres installed with screens at depth of approx. 2–4 m to measure groundwater interactions across supratidal and terrestrial zones. Table 1 summarises the installations. The transect exhibits vegetation conditions common of coastal wetlands in south-east Australia. Surface elevation range of the transect was 1.106 m Australian Height Datum (AHD), where the mangrove zone was positioned at 0.048 m AHD, saltmarsh at 0.301 m AHD, progressing to 1.154 m AHD for the terrestrial forest zone (Table 1).

The observed lithology across the transect demonstrate a clear progression in sediment composition from the intertidal zone to the terrestrial margin (Figure 2). Mangrove, ecotone and saltmarsh subsurface have shallow sequences of organic rich muds and silty clay, reflecting long-term accumulation of fine sediment under low-energy waterlogged conditions. These upper layers are generally thin and overlie more consolidated grey clays, indicating a relatively uniform and hydraulically

https://doi.org/10.5194/egusphere-2026-1398
Preprint. Discussion started: 8 April 2026

impermeable substrate close to the surface. Stratigraphy in the supratidal forest zones show profiles of thicker unsaturated zones with greater textural variability, suggesting increased terrestrial influence, episodic sediment deposition, and enhanced drainage. At the terrestrial zone beyond the influence of surface tidal inundation, the deepest log displays predominantly coarse sandy units interbedded with loams and minor clay layers, consistent with well-drained upland with more heterogeneous and coarser deposits, reflecting changing depositional environments and hydrological conditions across the landscape. Overall, there is horizontal layering which means that potential hydraulic pathways are more conductive horizontally than vertically.

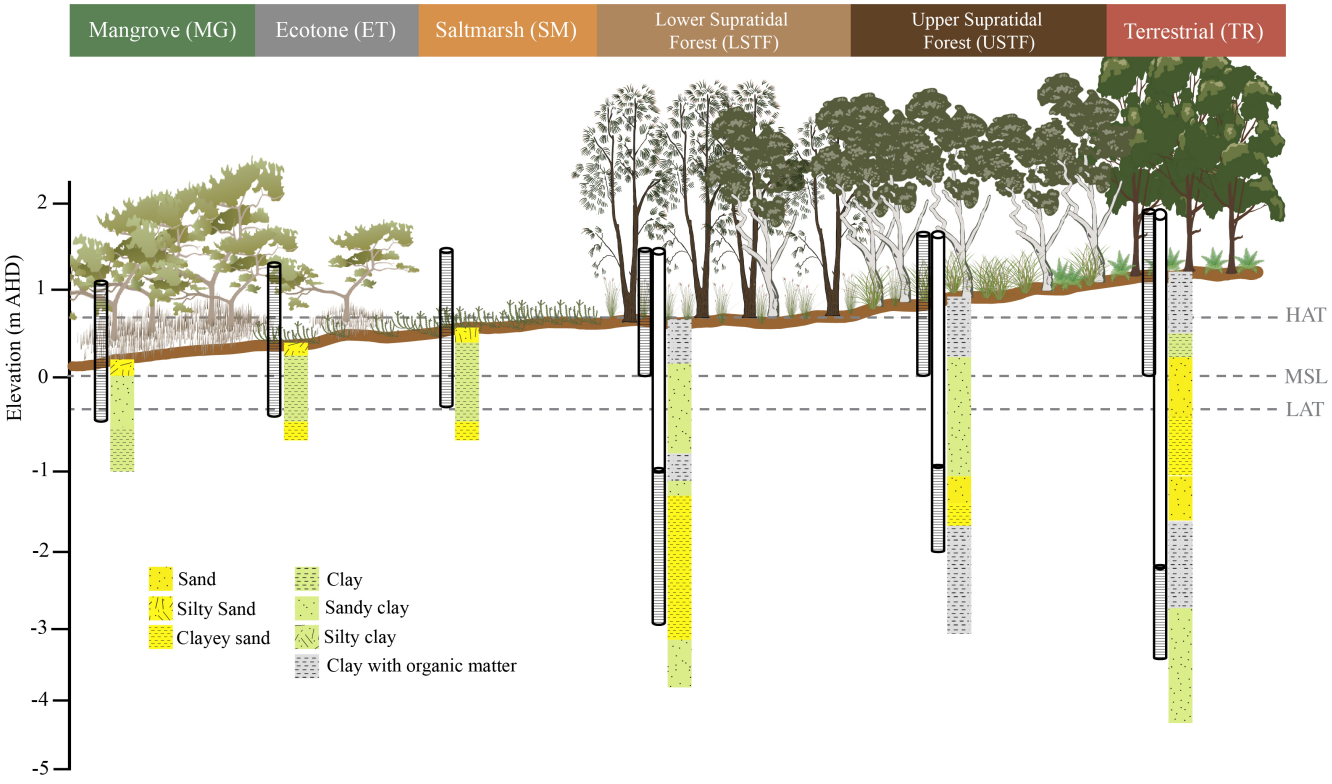

Figure 2. Transect showing surface and groundwater piezometre installations across vegetation communities. Grey sections represent screened intervals; solid white sections indicate solid pipe walls. Lithology is based on field observations from drilling logs (note that observational depths often exceeded piezometre installation depths). Vertical scale: 1 cm represents 1 m. Horizontal scale not to scale. Vegetation height not to scale. AHD: Australian Height Datum; HAT: Highest Astronomical Tide; MSL: Mean Sea Level; LAT: Lowest Astronomical Tide

3.2 Sediment characterisation

Sediment cores reveal systematic gradients in porewater salinity, grain size, and organic carbon across the vegetation transect (Figure 3). These parameters co-vary with landscape position, creating three distinct hydrogeological domains.

https://doi.org/10.5194/egusphere-2026-1398
Preprint. Discussion started: 8 April 2026

The mangrove, ecotone, and saltmarsh zones (MG, ET and SM) are characterised by persistently high porewater salinity (31–116 mS cm^{-1}), classifying these sediments as saline to hypersaline. Despite this similarity, textural differences influence salt retention: mangrove and ecotone profiles are sand-dominated at the surface but grade into silt-clay with depth, whereas the saltmarsh remains sand-dominated throughout yet exhibits the highest salinities recorded (up to 116 mS cm^{-1}), suggesting evaporative concentration overrides grain-size controls. Organic carbon is elevated across all three zones (6.7–21.0% in the upper 20 cm), peaking in the ecotone (21.0% at 10–20 cm) where moisture content also reaches 260%. Root systems penetrate throughout the upper 50 cm but remain confined to the low-permeability matrix. Grain-size-based estimates using the Kozeny-Carman equation suggest hydraulic conductivity values of approximately 10^{-8} to 10^{-9} m s^{-1} for these silty-clay dominated sediments.

Landward, the transition to supratidal forest (LSTF, USTF and TR) marks a shift toward sandier, more permeable sediments and lower, more variable salinity. The lower supratidal forest exhibits brackish-to-hypersaline conditions (15–60 mS cm^{-1}) with sand-dominated upper horizons overlying silt-clay at 0.5–1 m depth; organic carbon is moderate at the surface (6.7%) and decreases with depth, while root penetration is restricted (absent below 40 cm). The upper supratidal forest shows further improvement in drainage conditions, with salinity ranging from brackish to saline (7–33 mS cm^{-1}), sand content exceeding 80% at 80–100 cm, and continuous root presence throughout the profile. Shell material in both zones (60–90 cm) indicates intermittent marine deposition. Estimated hydraulic conductivity increases substantially to 10^{-5} to 10^{-6} m s^{-1} for these sandier deposits, reflecting enhanced vertical drainage relative to the intertidal zone.

Beyond tidal influence, the terrestrial zone exhibits the lowest salinities (0–7 mS cm^{-1}, fresh to slightly brackish) and a coarsening-downward texture (sand decreasing, clay increasing with depth). Both organic carbon and moisture decline steadily down-profile, contrasting with the intertidal pattern of surface enrichment. Fine roots penetrate continuously through the sediment profile. Estimated hydraulic conductivity of 10^{-5} to 10^{-6} m s^{-1} is comparable to the supratidal forest, consistent with the sand-dominated lithology and efficient vertical drainage that facilitates freshwater conditions at this landward position.

3.3 Subsurface bulk electrical conductivity

Subsurface bulk electrical conductivities (EC_B) from the ERT surveys on 21 February 2024 (ERT-1) and 12 June 2024 (ERT-2) were considered very similar, i.e., do not illustrate significant differences despite taken during periods of different hydrological conditions. For the lower supratidal forest zone in, EC_B measurements were greatest (10 mS cm^{-1}) within the upper 5 m of the subsurface and decreased with depth, with a slightly lower EC_B in June (8 mS cm^{-1}) (Figure 4). Similarly, the upper supratidal forest had higher EC_B near the wetland surface, which decreased with depth and laterally away from tidal influence towards the terrestrial zone. The terrestrial forest vegetation exhibited EC_B <3 mS cm^{-1}.

A strong lateral transition in subsurface salinity across the intertidal to supratidal gradient was observed in ERT-3 (5 September 2024). In the mangrove saltmarsh ecotone (ET) and saltmarsh (SM) zones of the transect, EC_B measurements were markedly higher than at inland sites, exceeding 14–16 mS cm^{-1} in the upper few metres of the subsurface (Figure 4). Elevated conductivities extended to greater depths beneath the SM zone, reflective of clays and suggesting long-term accumulation of salts from estuary inundation and limited freshwater dilution. Moving landward into the LSTF and USTF areas, EC_B de-

https://doi.org/10.5194/egusphere-2026-1398
Preprint. Discussion started: 8 April 2026

Table 1. Site data from monitoring locations along the transect, including coordinates (GDA2020 MGA Zone 56), elevation in metres Australian Height Datum (AHD), vegetation composition, and piezometre details. Groundwater pipe lengths reflect variations in depth of refusal across different vegetation communities. * represents a N/A value

Site	**Mangrove**	**Ecotone**	**Saltmarsh**	**Lower Supratidal Forest**	**Upper Supratidal Forest**	**Terrestrial**
ID	MG	ET	SM	LSTF	USTF	TR
Easting	349614.631	349649.269	349686.429	349735.245	349767.283	349839.729
Northing	6292791.502	6292817.315	6292778.373	6292767.215	6292740.93	6292682.267
Elevation (m AHD)	0.057	0.301	0.365	0.664	0.735	1.154
Vegetation (primary)	*Avicennia marina*	*Aegiceras corniculatum*	*Sarcocornia quinqueflora*	*Casuarina glauca*	*Melaleuca quinquenervia*	*Eucalyptus resinifera*
Vegetation (secondary)	*	*Sarcocornia quinqueflora*	*	*Juncus Kraussii*	*Lepidosperma gladiatum*	*Pteridium esculentum*
Groundwater piezometre screen depth (m AHD)	*	*	*	-1 to -3	-1 to -2	-2 to -3

creased rapidly both laterally and vertically, indicating less clays and more sand as well as freshwater. Overall, the ERT results highlight a pronounced subsurface salinity wedge that diminishes inland, mirroring the vegetation zonation observed across the wetland transect. Remarkably, at greater depths down to -30 m AHD, EC_B values below approx. 2 mS cm^{-1} across the site are consistent with freshwater-dominated sediments (Galazoulas et al., 2015; Lévesque et al., 2023).

3.4 Rainfall, water levels, inundation times, salinities and quality parameters

Figure 5 shows the daily and cumulative rainfall as well as surface and groundwater levels recorded over the monitoring period. The mean annual average rainfall for this study setting is 1,348 mm (Australian Government Bureau of Meteorology station *Gosford AWS*). A total of 2,954 mm of rainfall was recorded over the monitoring period (15 March 2024 to 17 December 2025), distributed across time as shorter periods of wet conditions (e.g., April to July 2024 and May to October 2025) as well as drier periods (e.g., October 2024 to January 2025). Mean and maximum daily rainfall were 4.6 mm/day and 156 mm/day.

Long-term average surface water table levels decreased with increasing elevation, ranging from 0.165 m AHD in mangrove to –0.002 m AHD in saltmarsh, before stabilising slightly in the higher elevation forested zones. While surface water table levels

https://doi.org/10.5194/egusphere-2026-1398
Preprint. Discussion started: 8 April 2026

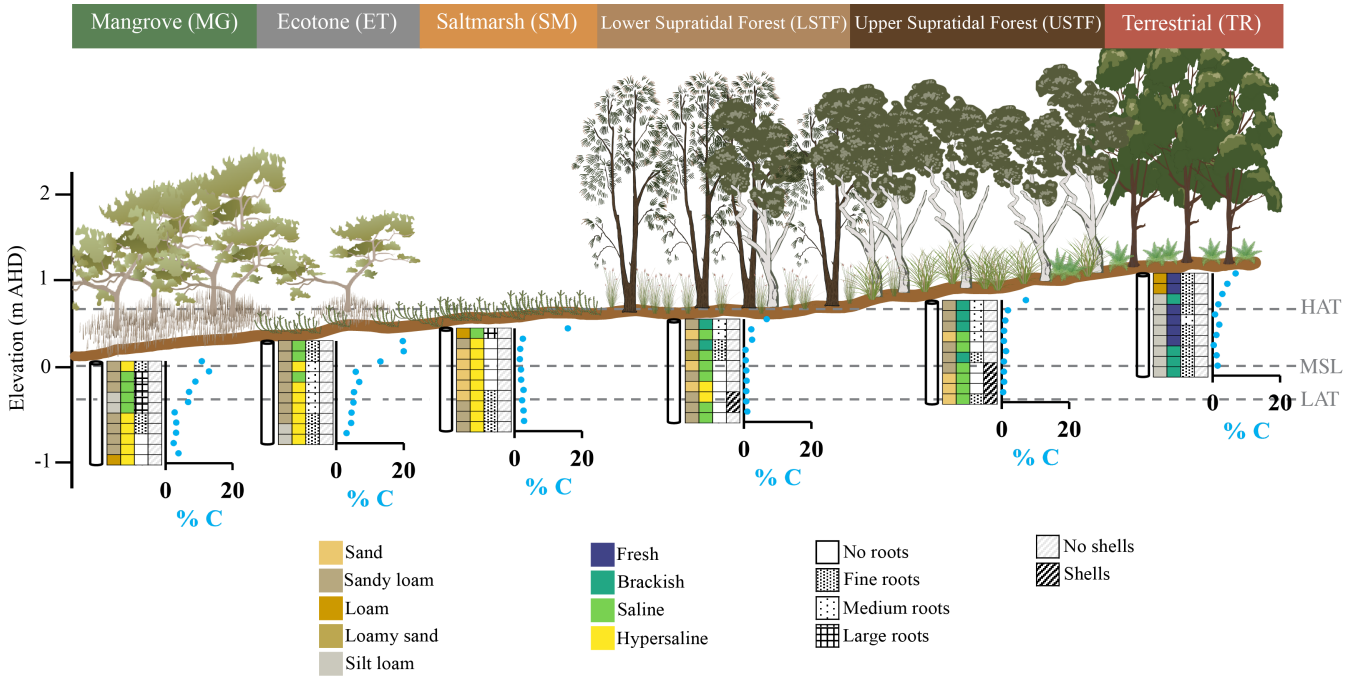

Figure 3. Transect showing core sampling locations in each vegetation community as indicated by a white cylinder. Cores samples were analysed in 10 cm increments, illustrated by black lines. Cores were analysed for sediment grain size (descriptors in beige colours), pore water salinity (descriptors in viridis colour scheme), presence of root and shell material (textured patterns), and organic carbon content (% C, axis representing carbon content values (blue) between 0% C and 20% C) to show changes in sediment characteristics. Note: Horizontal not to scale. Vegetation height not to scale. AHD: Australian Height Datum; HAT: Highest Astronomical Tide; MSL: Mean Sea Level; LAT: Lowest Astronomical Tide.

followed an expected elevational trend, groundwater measurements in the supratidal and terrestrial zones revealed relatively consistent water table elevations (0.025–0.085 m AHD) despite substantial differences in ground surface height (0.582 – 1.154 m AHD), suggesting the presence of a shallow groundwater system that is partially hydraulically decoupled from local surface topography.

Water levels in the intertidal zone followed regular tidal patterns, with MG and ET zones showing moderate correlation (0.61), indicating similar water level dynamics. Further inland, SM showed a strong correlation with ET (0.94), while SM and LSTF exhibited a slightly lower but still significant correlation (0.75). As elevation increased from SM to LSTF, water levels rose approximately 0.1 m on average. In the supratidal zones, LSTF water levels ranged up to 0.846 mAHD, strongly correlating with USTF (0.87). USTF had a maximum water level of 0.897 mAHD, with surface water and groundwater levels in this zone showing a very high correlation (0.94), but low correlation with MG (0.09). In the terrestrial zone, TR surface water fluctuated from -0.359 mAHD to 0.440 mAHD, with groundwater showing slightly smaller fluctuations. Heavy rainfall

https://doi.org/10.5194/egusphere-2026-1398
Preprint. Discussion started: 8 April 2026

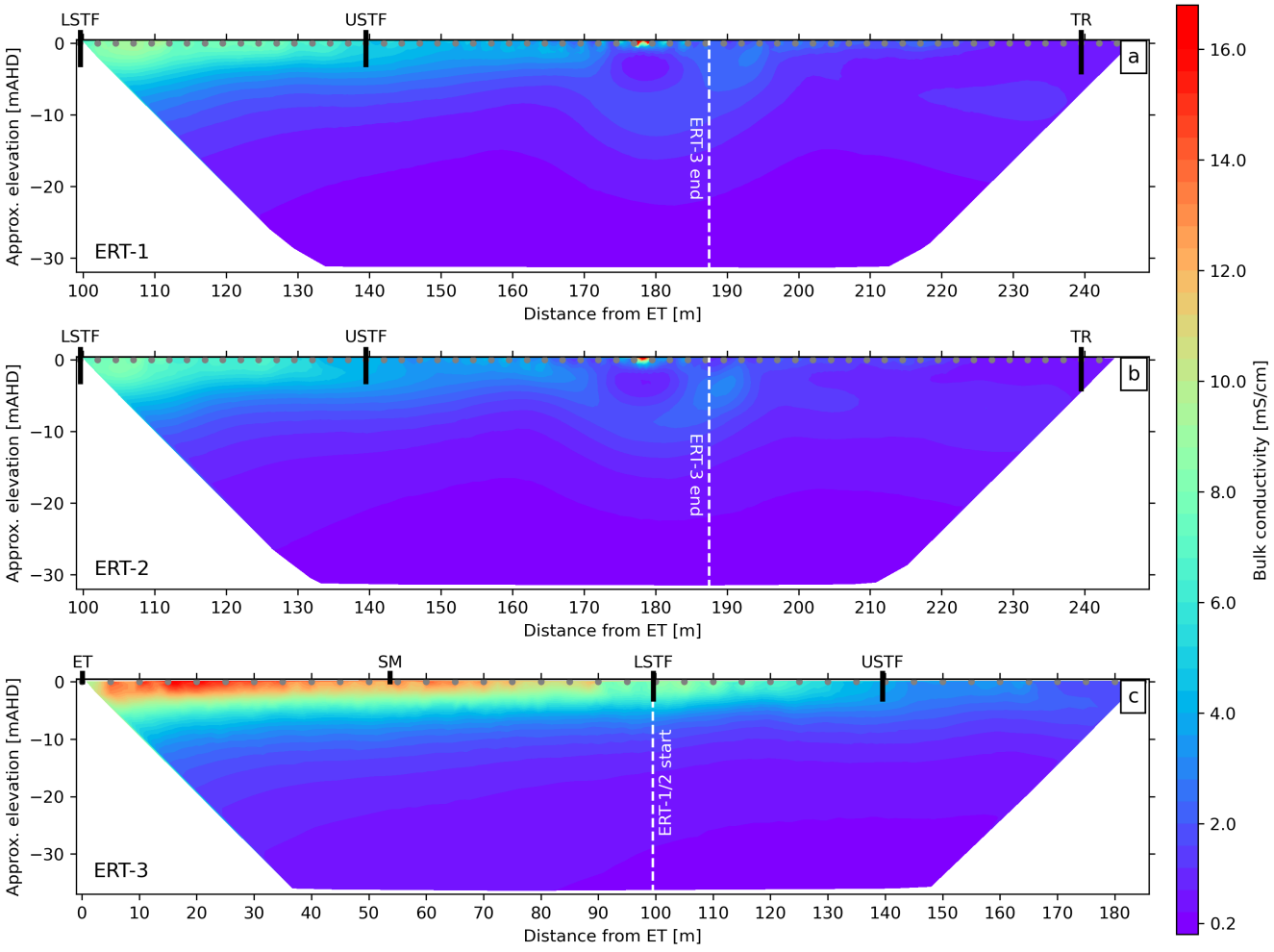

Figure 4. Electrical resistivity tomography (ERT) profiles expressed as bulk electrical conductivity EC_B (mS cm^{-1}) across the transect from monitoring locations ET to TR. ERT-1 (a) and ERT-2 (b) were acquired at the same location but different times, i.e., February and June 2024. ERT-3 (c) was measured starting from a different location but overlapping with ERT-1/2. The colour gradients represents EC_B, with higher EC_B values (in red) reflecting clay and/or saltwater and lower EC_B values (in dark blue) indicating sand and/or freshwater. ERT-1 and ERT-2 intended to inspect temporal changes, whereas ERT-3 was conducted to image beneath the mangrove and saltmarsh.

events in April caused water level peaks across all zones, notably in LSTF and USTF, where levels were amplified by spring tides.

Inundation frequency varied considerably across the different vegetated ecosystems, revealing complex patterns of hydroperiod that did not strictly follow surface elevation changes from intertidal to supratidal zones (Figure 6). Across the intertidal environment, mangrove was inundated 17.8% of the time, with a maximum water level of 58 cm above the surface over the observed time series (March 2024 – December 2025). Saltmarsh was inundated 4.6% of the time, which is, as expected, less

https://doi.org/10.5194/egusphere-2026-1398
Preprint. Discussion started: 8 April 2026

than mangrove. However, the greatest inundation frequency was observed for the mangrove–saltmarsh ecotone (71.5%), with a maximum water level of 59 cm above the surface, similar to mangrove. It is important to note the methodological approach of this study, which measures inundation resulting from combined tidal and rainfall influence (i.e. shallow groundwater). In the supratidal zone, the influence of rainfall was evident, with water levels observed above HAT on several occasions. This is likely due to rainfall accumulating in shallow depressions, diluting salinity, and floating on top of estuarine tidal water due to density effects. Within the supratidal zone, LSTF was inundated 28.7% of the time, followed by USTF (17.8%) and TR (5.1%), demonstrating a relationship with surface elevation that increases towards the terrestrial margin.

Electrical conductivity (EC) of water measured in the piezometre within the lower supratidal zone remained relatively stable at approximately 48 mS cm^{-1} throughout the monitoring period. In contrast, the surface installation recorded intermittent dry conditions, during which no valid measurements were obtained. During periods of tidal inundation or rainfall accumulation, surface EC varied between approximately 5 and 40 mS cm^{-1}. Lower values were associated with rainfall-driven dilution, whereas higher values reflected tidal influence. EC values close to zero indicate absence of water and dry conditions. At the upper supratidal location, piezometre EC values were lower but similarly stable at depth, averaging approximately 23 mS cm^{-1}. Surface EC ranged between roughly 10 and 30 mS cm^{-1}, increasing during tidal inundation and decreasing following rainfall events.

4 Discussion

4.1 Sediment characteristics across the wetland ecotone

Sediment cores reveal systematic textural gradients that establish the physical template for groundwater behaviour (Figures 3 and 2). The intertidal sequence (MG, ET, SM) comprises organic-rich silty clays and muddy sands with elevated organic carbon (6.7–21 % in the upper 20 cm), reflecting waterlogged, low-energy conditions typical of southeast Australian estuaries (Owers et al., 2022; Kelleway et al., 2017). These fine-grained layers host hypersaline groundwater (31–116 mS cm^{-1}), with saltmarsh exhibiting the highest salinities despite sand-dominated lithology—an anomaly suggesting evaporative concentration within the shallow profile overrides grain-size controls (Shen et al., 2018). Root systems penetrate throughout the upper 50 cm but remain bound within the low-permeability matrix (Conroy et al., 2025; Kelleway et al., 2016).

Landward, the transition to supratidal forests marks a shift toward sandier, more permeable sediments and progressively fresher groundwater. The lower supratidal forest exhibits sand-dominated upper horizons overlying silt–clay (0.5–1 m) with brackish-to-hypersaline groundwater (15–60 mS cm^{-1}), shell material at 70–90 cm indicating intermittent marine deposition (Owers et al., 2022; Lal et al., 2024), and restricted root penetration (absent below 40 cm). Further inland, the upper supratidal forest shows >80 % sand at 80–100 cm depth with lower salinity (7–33 mS cm^{-1}) and continuous root presence throughout the profile. The terrestrial zone comprises coarse sandy units with fresh groundwater (0–7 mS cm^{-1}), where fine roots penetrate continuously and both organic carbon and moisture decline steadily down-profile.

These textural contrasts impose distinct hydraulic domains across the transect. The multiple order-of-magnitude permeability contrast implies that vertical hydraulic conductivity in the intertidal zone may be 1–2 orders of magnitude lower than horizontal

https://doi.org/10.5194/egusphere-2026-1398
Preprint. Discussion started: 8 April 2026

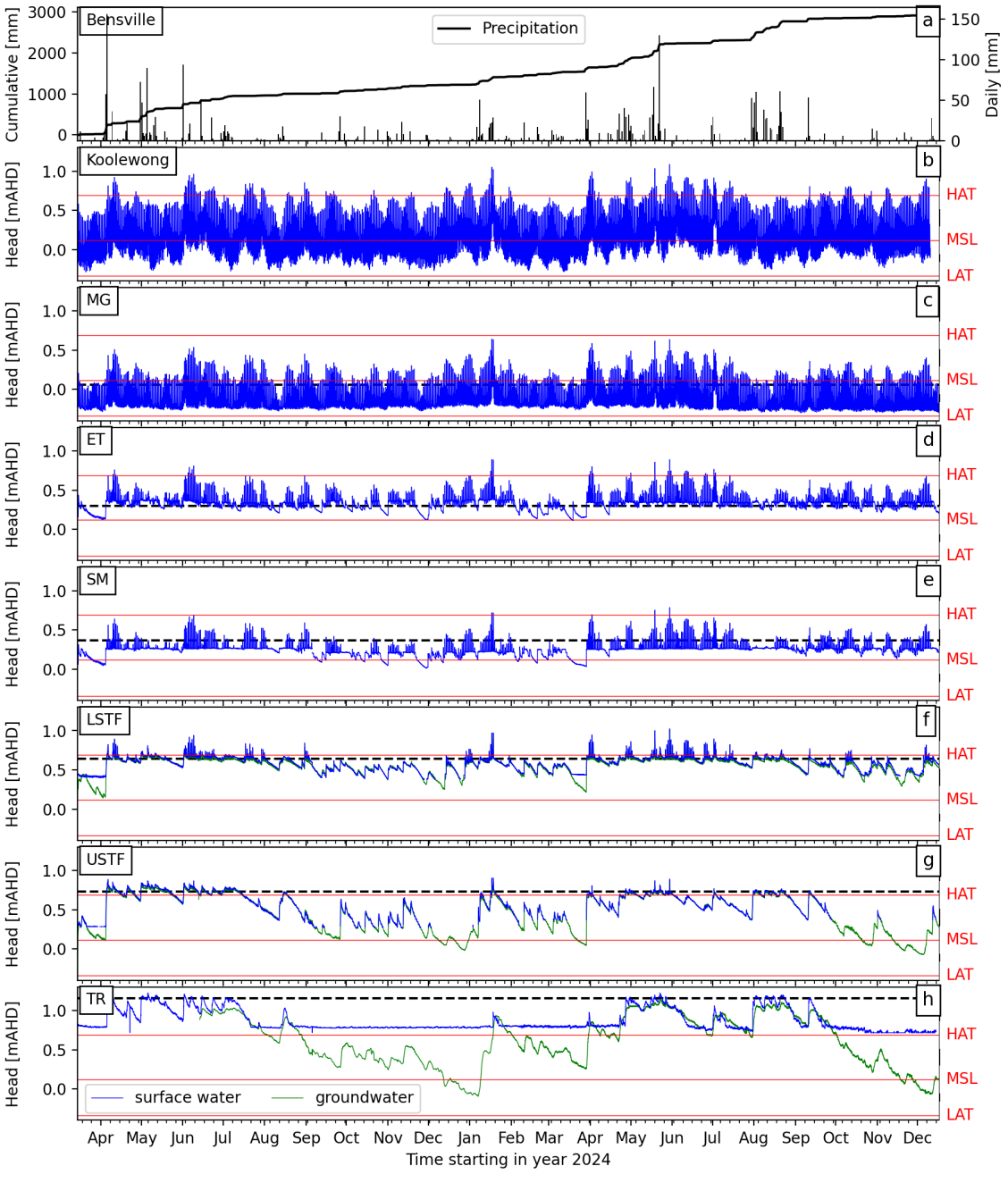

Figure 5. Hydraulic heads over time shown for locations: (a) Daily and cumulative rainfall (Kincumber, NSW), (b) estuary levels (Koolewong, NSW), (c) MG, (d) ET, (e) SM, (f) LSTF, (g) USTF and (h) TR. Surface water levels are shown in blue, while groundwater levels are shown in green for LSTF, USTF, and TR.

https://doi.org/10.5194/egusphere-2026-1398
Preprint. Discussion started: 8 April 2026

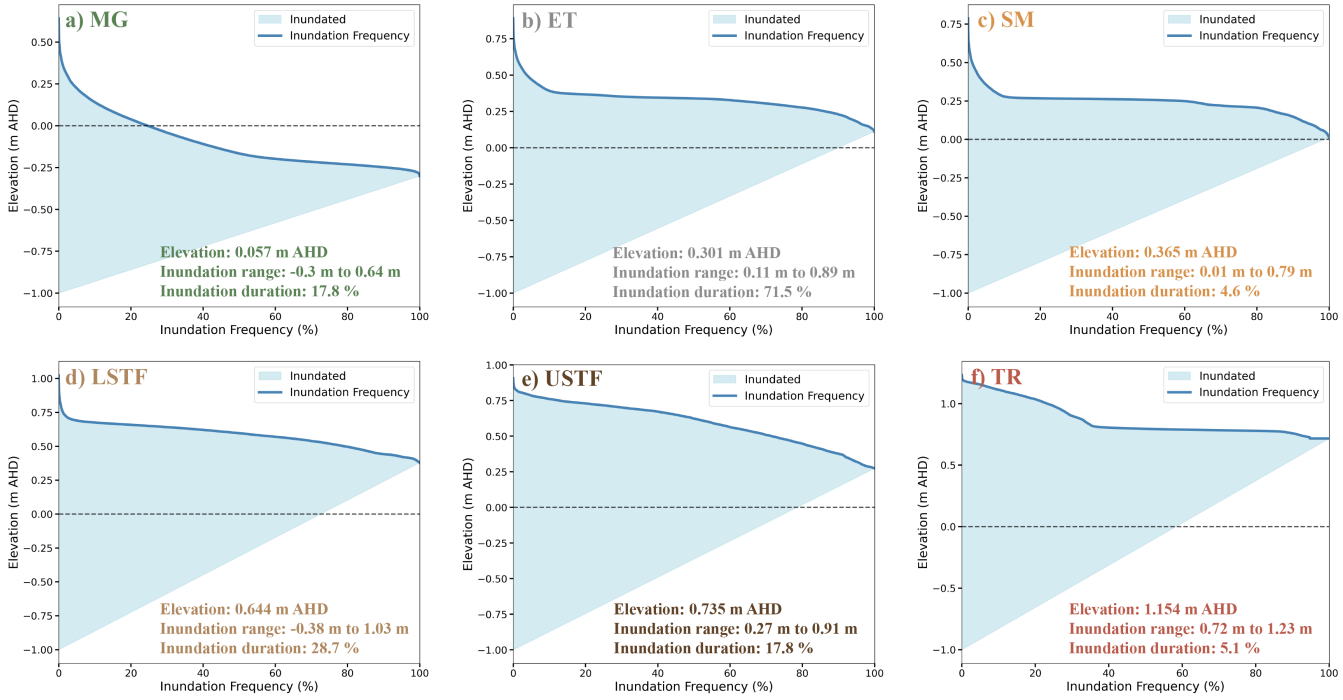

Figure 6. Inundation duration and frequency for surface water level measurements of each vegetation zone: (a) Mangrove (MG), (b) Saltmarsh (SM), (c) Mangrove-saltmarsh Ecotone (ET), (d) Lower Supratidal Forest (LSTF), (e) Upper Supratidal Forest (USTF), (f) Terrestrial forest (TR). Observed water levels recorded from March 2024 to December 2025.

values, consistent with effective anisotropy ratios (K_v/K_h) of 5 to 50 reported for layered coastal aquifers (Hemond and Fifield, 1982; Bakker and Bot, 2024). Such low-permeability surface layers are hypothesised to function as aquitards that restrict vertical saltwater intrusion (Etsias et al., 2021), promoting lateral retention of saline groundwater despite regular tidal inundation. Conversely, coarser supratidal and terrestrial sediments are inferred to facilitate enhanced vertical drainage and freshwater flushing, as evidenced by the landward salinity decline and deeper root penetration (to 100 cm at USTF, continuous through TR) (Redelstein et al., 2018). These estimated ranges align with measured values from comparable environments: fibrous salt-marsh peat typically ranges from 10^{-7} to 10^{-4} m s^{-1}, while marine clay values range from 10^{-11} to 10^{-9} m s^{-1} (Freeze and Cherry, 1979).

This sedimentary composition determines the degree of vertical hydraulic connectivity across the transect (Sadat-Noori et al., 2025). The intertidal zone functions as a low-permeability cap that isolates surface saline conditions from deeper horizons, while landward coarsening enables deeper freshwater recharge. Whether these sediment-controlled permeability contrasts generate the vertically stratified flow system suggested by ERT—wherein shallow saline retention coexists with deeper freshwater transmission—requires examination of the hydrodynamic data.

https://doi.org/10.5194/egusphere-2026-1398
Preprint. Discussion started: 8 April 2026

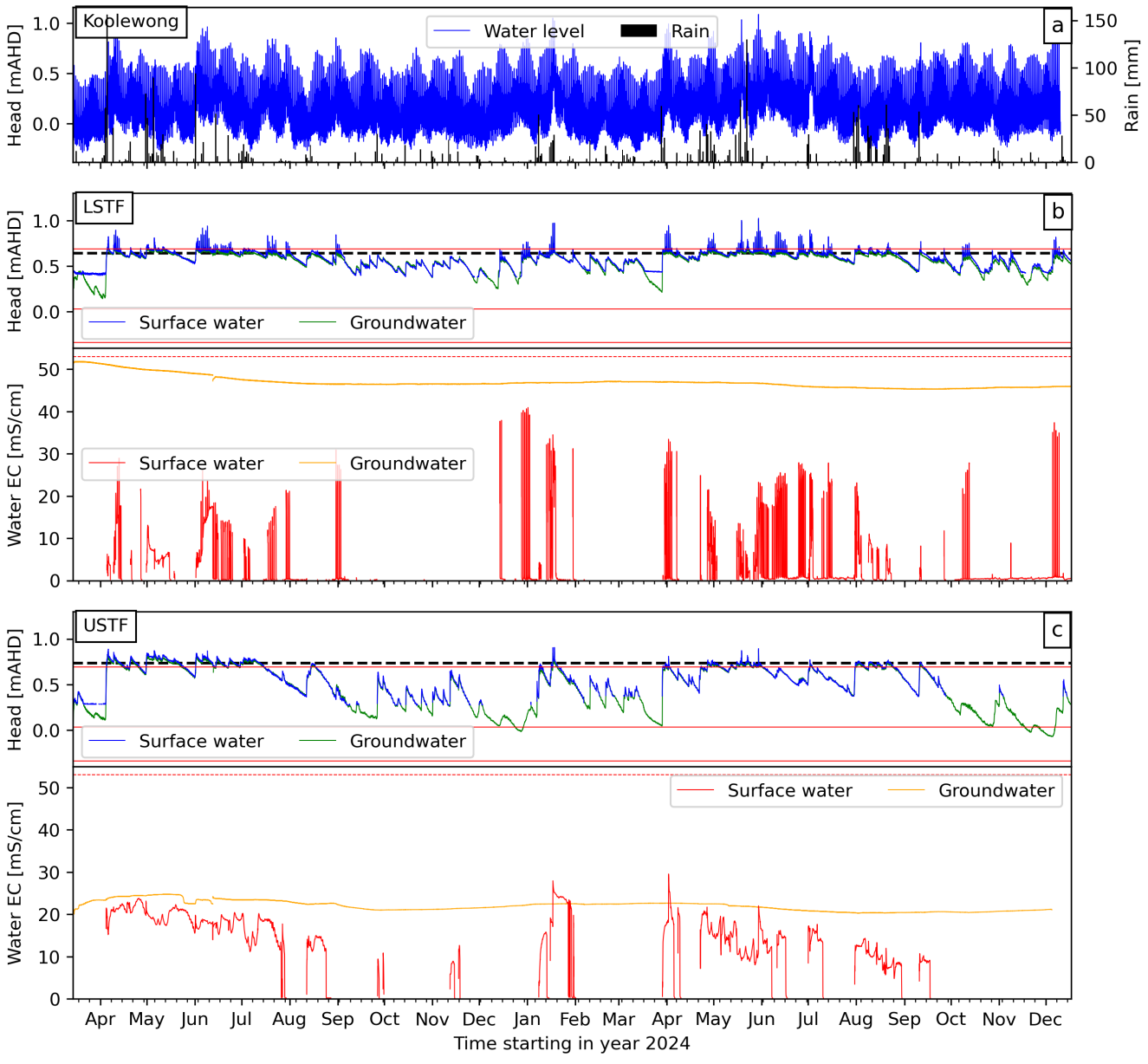

Figure 7. Hydraulic heads and water electrical conductivity (EC) at LSTF and USTF. (a) Estuary water levels and daily rainfall. (b) LSTF: hydraulic heads (surface water in blue, groundwater in green) and EC (surface water and groundwater). (c) USTF: hydraulic heads and EC as per (b).

It is important to note that these hydraulic interpretations are based on inferred relationships between sediment texture and permeability, rather than direct measurements. While grain-size distributions provide a basis for estimating K ranges using

https://doi.org/10.5194/egusphere-2026-1398
Preprint. Discussion started: 8 April 2026

empirical relationships (Hazen, 1892; Kozeny, 1927; Carman, 1997; Rosas et al., 2013), the absence of slug tests, permeameter measurements, or pumping tests means that absolute K values and anisotropy ratios remain uncertain. Consequently, descriptions of 'restricted vertical flow' and 'hydraulic decoupling' should be understood as working hypotheses consistent with observed sedimentary structure and hydrodynamic response, rather than quantitatively verified properties.

4.2 Water level and salinity dynamics

Surface water levels exhibit a progressive decoupling from tidal forcing across the vegetation gradient, transitioning from tide-dominated dynamics in the intertidal zone to rainfall-modulated hydrology in the supratidal and terrestrial zones (Figure 5). In the mangrove and ecotone zones, hydraulic heads closely track estuary tidal cycles, with inundation frequencies of 17.8% and 71.5%, respectively—somewhat consistent with microtidal estuarine dynamics given methodological differences as explained previously (Kumbier et al., 2021a, 2022).

Moving landward, the saltmarsh and supratidal forest zones display increasingly asynchronous water level fluctuations. Maximum observed heads frequently exceed Highest Astronomical Tide (HAT) during rainfall events (Figure 6), a phenomenon also documented across Australian supratidal forests (Kelleway et al., 2025). In these zones, rainfall accumulates in shallow depressions, dilutes surface salinity, and forms a perched freshwater lens "floating" atop estuarine tidal water due to density contrasts—indicating a shift from marine to meteoric dominance in surface hydrology. Inundation duration declines systematically across the gradient (LSTF: 28.7%, USTF: 17.8%, TR: 5.1%), yet the persistence of saturated conditions above HAT in the forested zones reveals that shallow groundwater storage is maintained by rainfall recharge rather than tidal pumping (cf. Sadat-Noori et al., 2025).

These surface dynamics establish the boundary conditions for vertical fluxes. While tidal and rainfall forcing generate rapid fluctuations in the upper sediments, the attenuation of these signals with depth suggests limited hydraulic connectivity between the dynamic shallow zone and deeper aquifer horizons.

Groundwater electrical conductivity (EC) exhibits pronounced vertical stratification consistent with this interpretation. Surface installations show high variability driven by tidal inundation and rainfall dilution, while deeper piezometres (2–4 m) remain comparatively stable. Rainfall events induce measurable freshening in shallow groundwater, but this dilution is rapidly attenuated with depth and confined to the upper sediment profile (<4 m). The absence of comparable freshening in deeper layers imaged by ERT indicates that vertical recharge is insufficient to displace the deeper saline domain, pointing to limited vertical connectivity within the fine-grained intertidal sediments.

This vertical decoupling reflects sediment-controlled hydraulic anisotropy, consistent with coastal systems elsewhere (Hemond and Fifield, 1982). The predominance of silt–clay layers in the shallow intertidal zone restricts vertical permeability relative to horizontal pathways, promoting stratification (Zhang, 1996) and limiting exchange between shallow (<4 m) and deeper groundwater. Consequently, surface salinity fluctuations remain hydraulically isolated from deeper regimes, which reflect longer-term balances between saltwater intrusion and lateral redistribution rather than vertical flushing. In contrast, sandier supratidal and terrestrial sediments facilitate greater vertical drainage, consistent with the fresher, less variable conditions observed landward.

https://doi.org/10.5194/egusphere-2026-1398
Preprint. Discussion started: 8 April 2026

The lateral transition from high bulk EC intertidal sediments to low-EC terrestrial deposits creates a landward-diminishing salinity wedge (Figure 4). Laterally continuous fine-grained layers retain saline groundwater within the shallow intertidal domain while restricting downward salinisation, whereas landward coarsening enhances freshwater flushing. Thus, sediment composition—specifically the subsurface sediment structure—exerts first-order control on subsurface salinity structure, maintaining persistent shallow saline conditions over deeper, terrestrially influenced freshwater.

4.3 Surface-groundwater interactions across the vegetated wetland

Hydraulic head measurements reveal that shallow groundwater within the intertidal and supratidal zones flows laterally toward the estuary, driven by tidal pumping, rainfall inputs, and topographic gradients (Figure 5). Surface water EC fluctuates with tidal inundation and rainfall dilution, consistent with this horizontal drainage pattern toward the estuarine boundary (Figure 7). These dynamic signals attenuate rapidly with depth (Prihantono et al., 2023), such that shallow saline groundwater (< 5 m) persists directly over a deeper brackish-to-fresh groundwater system (Figure 4) that shows minimal response to surface salinisation or episodic flushing (Figure 7b,c).

This vertical stratification—saline shallow groundwater overlying a fresh deeper aquifer—inverts the classical coastal hydrogeological model of a freshwater lens floating atop saline water (Jiao and Post, 2019a; Sadat-Noori et al., 2025). Regular tidal inundation delivers marine water to the surface, and density gradients should favour downward intrusion (e.g., Sherif and Singh, 1996; Jiao and Post, 2019a). While shallow brackish groundwater drains horizontally toward the estuary (Figure 5), the persistence of fresh conditions at depth—particularly over the millennial timescales of wetland evolution (Rogers et al., 2019; Allen, 2000)—cannot be maintained by lateral drainage alone. The absence of deep salinisation despite continuous marine forcing requires an active freshwater flushing mechanism to prevent downward saltwater migration into the lower aquifer.

We infer that recharge within the permeable terrestrial and supratidal zones generates deeper lateral groundwater flow beneath the wetland toward the estuarine boundary. Low-permeability silt–clay layers within the intertidal zone restrict vertical connectivity, promoting hydraulic anisotropy (Zhang, 1996) that hydraulically isolates the deep aquifer from surface salinisation while facilitating lateral transport of terrestrially derived freshwater beneath the saline shallow domain. The groundwater system thus behaves as a vertically stratified aquifer-aquitard sequence: the shallow zone drains horizontally toward the estuary under tidal and rainfall influence, while the deeper zone is governed by regionally recharged freshwater flowing laterally beneath the wetland.

Figure 8 synthesises these processes into a coherent framework, though the deep structural interpretation remains hypothetical. While ERT provides spatially continuous bulk EC constraints, the inferred hydrostratigraphic composition, hydraulic gradients, and terrestrial recharge pathway lack direct verification through deep borehole logging or depth-resolved salinity profiling. The absence of direct hydraulic conductivity measurements represents a key limitation; although sediment texture and hydrodynamic response support the proposed stratification, quantification of K_v/K_h ratios and absolute permeability values awaits future field testing. Nevertheless, our conceptualisation aligns with the processes described by Guimond (2025), providing additional detail on shallow hydrogeological structure. These working hypotheses warrant targeted investigation to confirm the proposed lateral flow dynamics and stratified aquifer configuration in other low-energy estuarine wetlands.

https://doi.org/10.5194/egusphere-2026-1398
Preprint. Discussion started: 8 April 2026

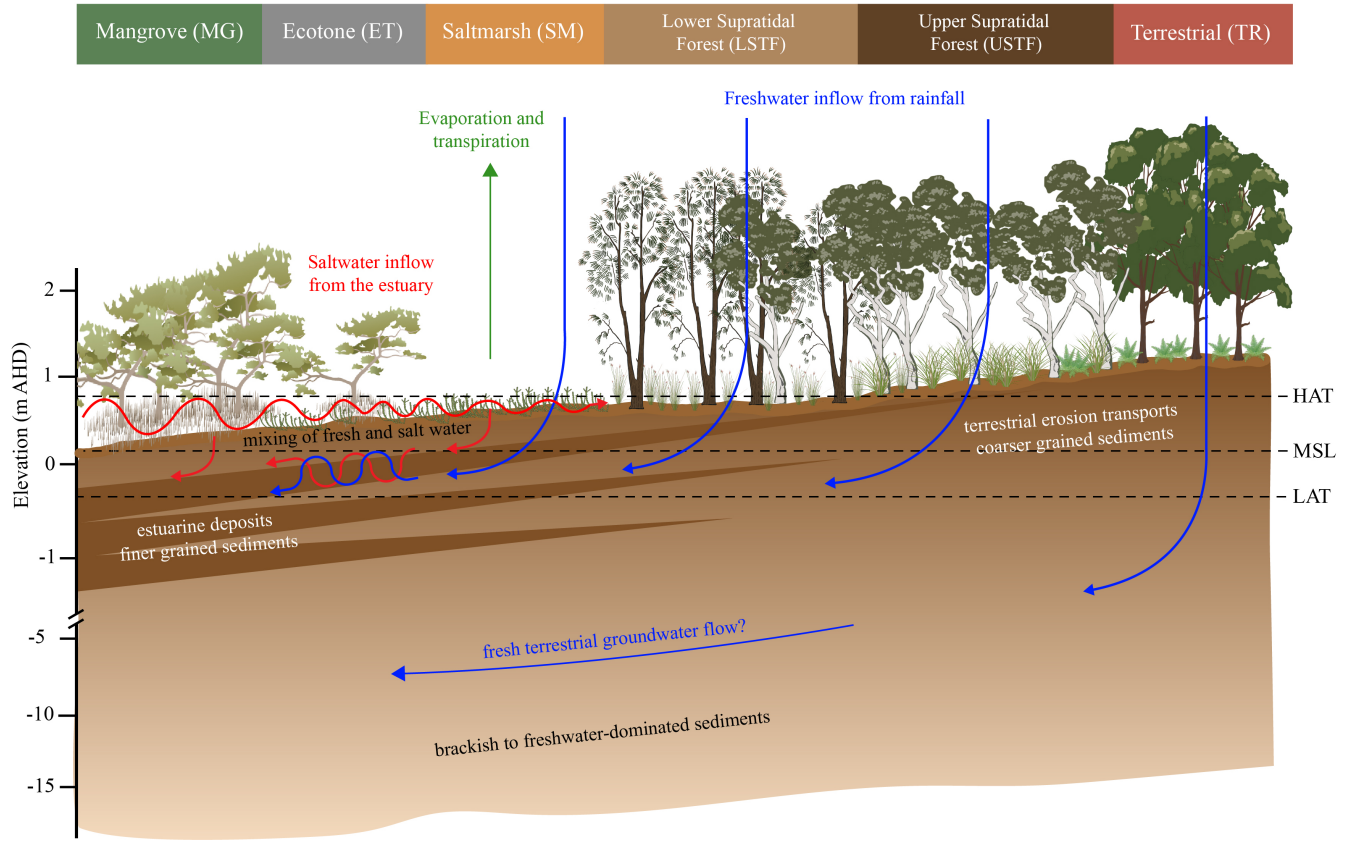

Figure 8. Conceptual model of sediment-controlled groundwater stratification across the wetland transect. The upper panel shows vegetation zonation. The lower panel presents the interpreted subsurface composition: shallow saline groundwater is retained within fine-grained intertidal sediments and drains laterally toward the estuary, while deeper freshwater flows landward-to-estuary beneath the saline wedge, recharged from the permeable terrestrial zone (Figure 4). Vertical hydraulic anisotropy imposed by silt–clay layers restricts downward flow and facilitates horizontal mixing of freshwater from precipitation and salt water from tidal inundation. This illustrates a stratified aquifer–aquitard sequence that decouples surface and deep hydrological processes.

4.4 Implications for hydrological process understanding within vegetated coastal wetlands

Our findings indicate that the classical freshwater-lens / seawater-wedge conceptualisation commonly applied in coastal hydrogeology (e.g., Jiao and Post, 2019a) inadequately describes barrier-protected coastal wetlands characterised by low wave energy and progressive fine-sediment accretion. In such settings, accumulated silts, clays and organic matter impose strong vertical permeability contrasts that promote hydraulic stratification and vertical decoupling between shallow saline groundwater and deeper freshwater bodies. We therefore propose a refined conceptual model for low-energy estuarine ecotones in Figure 8 that explicitly integrates sedimentary evolution, hydraulic anisotropy, and potentially terrestrially recharged deep groundwater flow. While the shallow stratification (0–5 m) is strongly supported by the sedimentary and hydrological evidence presented here,

https://doi.org/10.5194/egusphere-2026-1398
Preprint. Discussion started: 8 April 2026

the deep hydrogeological composition aligns with previous findings Guimond (2025) but remains hypothetical and requires validation through drilling, stratigraphic logging, and depth-resolved hydraulic and salinity measurements.

The vertically stratified composition exerts direct influence on vegetation zonation and ecosystem functioning. We infer this stratification reflects sediment-controlled hydraulic anisotropy, though direct permeability measurements are needed to quantify vertical to horizontal K ratios. Mangrove and saltmarsh communities align with intertidal zones where fine-grained sediments retain elevated shallow salinity, while the sandier supratidal and terrestrial zones—characterised by lower bulk EC and stable freshwater conditions at depth—support vegetation (e.g., *Casuarina*, *Melaleuca*, *Eucalyptus*) consistent with reduced marine influence. Rather than passive occupants of tidal elevation zones, these vegetation assemblages may serve as ecological indicators of subsurface hydrogeological composition, effectively mapping the lateral extent of the saline wedge and the vertical accessibility of underlying freshwater resources.

This hydraulic stratification may also influence carbon preservation in intertidal sediments. By restricting vertical drainage, low-permeability silt-clay layers maintain waterlogged, anoxic conditions that inhibit organic matter decomposition (e.g., Owers et al., 2022). The persistence of hypersaline, saturated conditions in the saltmarsh (Figure 3)—despite sandy matrix texture—suggests that the overlying clay cap acts as an aquitard, preventing oxygen penetration and supporting the high carbon densities (up to 21% OC) observed. While we attribute this salt retention to restricted drainage, we cannot exclude evaporative concentration as a contributing process without isotopic or evaporation rate data (e.g., Li et al., 2023). Conversely, enhanced drainage in sandy supratidal zones may limit carbon accumulation despite high vegetation productivity. The proposed model thus links sedimentary composition not only to salinity distribution but to the long-term carbon sequestration capacity of these ecosystems.

Critical uncertainties remain regarding how vegetation accesses water within this stratified system (Kelleway et al., 2025; Sadat-Noori et al., 2025). Mangrove and saltmarsh colonisation of the intertidal zone indicates physiological tolerance of persistent shallow salinity, likely relying on the dynamic mixing zone within the upper sediment profile. The shift to supratidal forests and terrestrial vegetation signals access to less saline conditions, potentially mediated by deep root penetration to the freshwater horizon or exploitation of transient rainfall dilution at the surface. Ecosystem resilience may therefore depend on the degree of hydraulic connectivity between shallow saline root zones and deeper freshwater sources—a question requiring direct investigation of root distribution, water sourcing (e.g., isotopic analysis), and the hydraulic properties governing vertical versus lateral water uptake.

Our 20-month dataset captures hydrological transients but cannot resolve decadal to centennial adjustments to sea-level rise. The resilience of deep freshwater inferred from short-term stability (Figure 7) assumes stationary boundary conditions. Accelerated sea-level rise may compress the saline wedge landward faster than sediment accumulation can compensate, or alter recharge patterns in the terrestrial zone. The conceptual model (Figure 8) should therefore be viewed as a snapshot of contemporary conditions under anomalously high rainfall, rather than a prediction of future equilibrium states. Whether deeper freshwater can persist beneath intensified marine influence will depend on the strength of terrestrial recharge and the integrity of the stratified aquifer structure. If recharge remains sufficient, deeper freshwater may continue to exert a buffering influence; if not, progressive subsurface salinisation could alter vegetation composition and zonation over time (Guimond, 2025).

https://doi.org/10.5194/egusphere-2026-1398
Preprint. Discussion started: 8 April 2026

Advancing process understanding in such systems is essential for predicting groundwater dynamics and wetland ecosystem resilience under accelerating sea-level rise.

5 Conclusions

This study integrates electrical resistivity tomography imaging, hydrological monitoring, and sedimentological characterisation (0–1 m cores) to investigate groundwater–salinity dynamics of a coastal vegetated wetland within a low-energy, barrier estuary. The results reveal a pronounced lateral and vertical salinity structure, with shallow elevated bulk conductivities confined to fine-grained intertidal sediments and a landward-diminishing salinity wedge. Although rainfall and tidal forcing dynamically modify shallow groundwater salinity, this variability attenuates rapidly with depth, indicating limited vertical connectivity imposed by low-permeability silts and clays.

Beneath the saline shallow subsurface, electrical conductivity values indicate freshwater-dominated sediments. This vertical contrast departs from the classical homogeneous, density-driven coastal aquifer model. Instead, the system reflects a sediment-controlled, hydraulically stratified composition in which progressive estuarine infilling and fine-sediment accretion impose strong vertical permeability contrasts. Rainfall-driven flushing is largely confined to the upper sediments, and no substantial downward propagation of saline porewater is evident. The persistence of deeper freshwater is consistent with terrestrial recharge within permeable supratidal and upland deposits, potentially generating lateral groundwater flow toward the estuarine boundary that may act as a hydraulic barrier. Deep drilling is required to verify whether this deep freshwater lens is hydraulically active or represents relic/partially saturated deposits.

This vertically stratified configuration is expressed through vegetation zonation, with distinct community assemblages that may serve as surface indicators of subsurface hydrogeological composition. Mangrove and saltmarsh colonisation of the intertidal zone indicates persistent shallow salinity within low-permeability sediments, while the landward transition to supratidal forests (*Casuarina*, *Melaleuca*) and terrestrial vegetation (*Eucalyptus*) signals increasing accessibility of deeper freshwater resources. Rather than representing communities maintained by fixed salinity thresholds, these vegetation boundaries effectively map the lateral extent of the saline wedge and the vertical partitioning of water sources, raising critical questions regarding root-zone connectivity and ecosystem resilience under variable recharge conditions.

Under relative sea-level rise, shifts in the balance between marine influence, terrestrial recharge, and sediment-controlled permeability may alter the thickness and extent of the shallow saline domain, with implications for vegetation distribution and carbon storage. We therefore propose a refined conceptual model for barrier-protected, low-energy estuarine ecotones in which sedimentary evolution and hydraulic anisotropy govern the coexistence of shallow marine influence and deeper freshwater flow. While strongly supported by the integrated evidence presented here, this framework remains hypothesis-driven and requires validation through drilling, stratigraphic logging, and depth-resolved hydraulic and salinity measurements. Advancing process understanding in such settings is essential for predicting groundwater dynamics and ecosystem resilience under accelerating sea-level rise.

https://doi.org/10.5194/egusphere-2026-1398
Preprint. Discussion started: 8 April 2026

Data availability. Data will be made publicly available after this manuscript is accepted.

Author contributions. The idea for this research was conceived equally by CJO and GCR. The manuscript is based on an Honours thesis written by RM. All authors conducted field work in Bensville, NSW, Australia. RM analysed the dataset and wrote the first draft under supervision of CJO and GCR. CJO and GCR updated the dataset and wrote the manuscript.

Competing interests. At least one of the (co-)authors is a member of the editorial board of Hydrology and Earth System Sciences.

Acknowledgements. We thank Murray Kendall and others who supported field and laboratory work. Dr Jeff Kelleway and A/Prof Danielle Verdon-Kidd who examined the Honours thesis of RM and provided helpful suggestions toward publication of the thesis. Kimi AI was used to check grammar and curate the language.

https://doi.org/10.5194/egusphere-2026-1398
Preprint. Discussion started: 8 April 2026

References

Adame, M. F., Kelleway, J., Krauss, K. W., Lovelock, C. E., Adams, J. B., Trevathan-Tackett, S. M., Noe, G., Jeffrey, L., Ronan, M., Zann, M., Carnell, P. E., Iram, N., Maher, D. T., Murdiyarso, D., Sasmito, S., Tran, D. B., Dargusch, P., Kauffman, J. B., and Brophy, L.: All tidal wetlands are blue carbon ecosystems, BioScience, 0, 1–16, https://doi.org/10.1093/biosci/biae007, 2024.

Allen, J. R.: Morphodynamics of Holocene salt marshes: a review sketch from the Atlantic and Southern North Sea coasts of Europe, Quaternary Science Reviews, 19, 1155–1231, https://doi.org/10.1016/s0277-3791(99)00034-7, 2000.

Atlas of Living, A.: Species: Juncus kraussii (Sea Rush), https://id.biodiversity.org.au/node/apni/2900900, 2007.

Bakker, M. and Bot, B.: The Effective Vertical Anisotropy of Layered Aquifers, Groundwater, 63, 68–75, https://doi.org/10.1111/gwat.13432, 2024.

Barbier, E. B., Hacker, S. D., Kennedy, C., Koch, E. W., Stier, A. C., and Silliman, B. R.: The value of estuarine and coastal ecosystem services, Ecological Monographs, 81, 169–193, https://doi.org/10.1890/10-1510.1, 2011.

Bear, J., Cheng, A. H.-D., Sorek, S., Ouazar, D., and Herrera, I.: Seawater Intrusion in Coastal Aquifers: Concepts, Methods and Practices, Springer Dordrecht, ISBN 978-0-7923-5573-1, https://doi.org/10.1007/978-94-017-2969-7, hardcover ISBN: 978-0-7923-5573-1, Softcover ISBN: 978-90-481-5172-1, eBook ISBN: 978-94-017-2969-7, 1999.

Beck, H. E., McVicar, T. R., Vergopolan, N., Berg, A., Lutsko, N. J., Dufour, A., Zeng, Z., Jiang, X., Van Dijk, A. I., and Miralles, D. G.: High-resolution (1 km) Köppen-Geiger maps for 1901–2099 based on constrained CMIP6 projections, Scientific data, 10, 724, https://doi.org/10.1038/s41597-023-02549-6, 2023.

Blanchy, G., Saneiyan, S., Boyd, J., McLachlan, P., and Binley, A.: ResIPy, an intuitive open source software for complex geoelectrical inversion/modeling, Computers & Geosciences, 137, 104 423, https://doi.org/10.1016/j.cageo.2020.104423, 2020.

Boyd, R., Dalrymple, R., and Zaitlin, B.: Classification of clastic coastal depositional environments, Sedimentary Geology, 80, 139–150, https://doi.org/10.1016/0037-0738(92)90037-r, 1992.

Cahoon, D. R., Hensel, P. F., Spencer, T., Reed, D. J., McKee, K. L., and Saintilan, N.: Coastal wetland vulnerability to relative sea-level rise: wetland elevation trends and process controls, in: Wetlands and natural resource management, pp. 271–292, Springer, 2006.

Carman, P.: Fluid flow through granular beds, Chemical Engineering Research and Design, 75, S32–S48, https://doi.org/10.1016/s0263-8762(97)80003-2, 1997.

Conroy, B. M., Kelleway, J. J., and Rogers, K.: Root productivity contributes to carbon storage and surface elevation adjustments in coastal wetlands, Plant and Soil, 513, 605–631, https://doi.org/10.1007/s11104-025-07204-0, 2025.

Custodio, E. and Bruggeman, G.: Groundwater Problems in Coastal Areas, UNESCO, Paris, studies and reports in hydrology, No. 45. ISBN: 92-3-102414-0, 1987.

DCCEEW, N.: Central Coast Climate Change Snapshot, https://www.climatechange.environment.nsw.gov.au/sites/default/files/2025-08/CCSnapshotN22025.pdf.

Etsias, G., Hamill, G. A., Águila, J. F., Benner, E. M., McDonnell, M. C., Ahmed, A. A., and Flynn, R.: The impact of aquifer stratification on saltwater intrusion characteristics. Comprehensive laboratory and numerical study, Hydrological Processes, 35, https://doi.org/10.1002/hyp.14120, 2021.

Ewel, K., Twilley, R., and Ong, J.: Different kinds of mangrove forests provide different goods and services, Global Ecology & Biogeography Letters, 7, 83–94, https://doi.org/10.2307/2997700, 1998.

https://doi.org/10.5194/egusphere-2026-1398
Preprint. Discussion started: 8 April 2026

Fernandez Winzer, L., Carnegie, A. J., Pegg, G. S., and Leishman, M. R.: Impacts of the invasive fungus Austropuccinia psidii (myrtle rust) on three Australian Myrtaceae species of coastal swamp woodland, Austral Ecology, 43, 56–68, https://doi.org/10.1111/aec.12534, 2018.

Freeze, R. A. and Cherry, J. A.: Groundwater, Prentice-Hall, Englewood Cliffs, NJ, ISBN 978-0-13-365312-0, 1979.

Friess, D. A., Rogers, K., Lovelock, C. E., Krauss, K. W., Hamilton, S. E., Lee, S. Y., Lucas, R., Primavera, J., Rajkaran, A., and Shi, S.: The state of the world's mangrove forests: past, present, and future, Annual Review of Environment and Resources, 44, 89–115, https://doi.org/10.1146/annurev-environ-101718-033302, 2019.

Galazoulas, E. C., Mertzanides, Y. C., Petalas, C. P., and Kargiotis, E. K.: Large Scale Electrical Resistivity Tomography Survey Correlated to Hydrogeological Data for Mapping Groundwater Salinization: A Case Study from a Multilayered Coastal Aquifer in Rhodope, Northeastern Greece, Environmental Processes, 2, 19–35, https://doi.org/10.1007/s40710-015-0061-y, 2015.

Glamore, W., Rayner, D., and Rahman, P.: Water Research Laboratory, Tech. rep., 2016.

Guimond, J. A.: The overlooked role of terrestrial groundwater in coastal wetland resilience, Nature Water, 3, 364–366, https://doi.org/10.1038/s44221-025-00406-x, 2025.

Harvey, N. and Caton, B.: Coastal Management in Australia, 2003.

Hazen, A.: Some physical properties of sands and gravels, with special reference to their use in filtration, Tech. rep., Massachusetts State Board of Health, Boston, annual Report, 1892.

Heiri, O., Lotter, A. F., and Lemcke, G.: Loss on ignition as a method for estimating organic and carbonate content in sediments: reproducibility and comparability of results, Journal of Paleolimnology, 25, 101–110, https://doi.org/10.1023/A:1008119611481, 2001.

Hemond, H. F. and Fifield, J. L.: Subsurface flow in salt marsh peat: A model and field study1, Limnology and Oceanography, 27, 126–136, https://doi.org/10.4319/lo.1982.27.1.0126, 1982.

Jiao, J. and Post, V.: Coastal Hydrogeology, Cambridge University Press, ISBN 9781107030596, https://doi.org/10.1017/9781139344142, 2019a.

Jiao, J. and Post, V.: Coastal Hydrogeology, Cambridge University Press, Cambridge, ISBN 978-1-107-03059-6, https://doi.org/10.1017/9781139344142, 2019b.

Kelleway, J., Noe, G. B., Krauss, K. W., Brophy, L., Connor, W. H., Duberstein, J. A., Friess, D. A., Gedan, K., White Jr, E., Adame, M. F., et al.: Beyond the mangroves: a global synthesis of tidal forested wetland types, drivers and future information needs, https://doi.org/10.31223/X5ZF2B, in review.

Kelleway, J. J., Saintilan, N., Macreadie, P. I., and Ralph, P. J.: Sedimentary Factors are Key Predictors of Carbon Storage in SE Australian Saltmarshes, Ecosystems, 19, 865–880, https://doi.org/10.1007/s10021-016-9972-3, 2016.

Kelleway, J. J., Saintilan, N., Macreadie, P. I., Baldock, J. A., and Ralph, P. J.: Sediment and carbon deposition vary among vegetation assemblages in a coastal salt marsh, Biogeosciences, 14, 3763–3779, https://doi.org/10.5194/bg-14-3763-2017, publisher: Copernicus GmbH, 2017.

Kelleway, J. J., Adame, M. F., Gorham, C., Bratchell, J., Serrano, O., Lavery, P. S., Owers, C. J., Rogers, K., Nagel-Tynan, Z., and Saintilan, N.: Carbon Storage in the Coastal Swamp Oak Forest Wetlands of Australia, chap. 18, pp. 339–353, American Geophysical Union (AGU), ISBN 9781119639305, https://doi.org/https://doi.org/10.1002/9781119639305.ch18, 2021a.

Kelleway, J. J., Adame, M. F., Gorham, C., Bratchell, J., Serrano, O., Lavery, P. S., Owers, C. J., Rogers, K., Nagel-Tynan, Z., and Saintilan, N.: Carbon Storage in the Coastal Swamp Oak Forest Wetlands of Australia, in: Wetland Carbon and Environmental Management, edited by Krauss, K. W., Zhu, Z., and Stagg, C. L., vol. 267 of *Gephysical Monograph*, pp. 339–353, 1 edn., https://doi.org/10.1002/9781119639305.ch18, 2021b.

https://doi.org/10.5194/egusphere-2026-1398
Preprint. Discussion started: 8 April 2026

Kelleway, J. J., Gorham, C., Trevathan-Tackett, S. M., Palacios, M., Serrano, O., Lavery, P. S., Nagel-Tynan, Z., Conroy, B. M., Bendall-Pease, G., Rigney, S. D., Deutscher, N. M., Hughes, M. G., Carvalho, R. C., Owers, C. J., Jones, A. R., Russell, S. K., Planque, C., Saintilan, N., and Rogers, K.: Inundation and salinity regimes support blue carbon conditions in Australian temperate supratidal forests, Ecological Applications, 35, e70 123, https://doi.org/https://doi.org/10.1002/eap.70123, 2025.

Kozeny, J.: Über kapillare Leitung des Wassers im Boden (Aufstieg, Versickerung und Anwendung auf die Bewässerung), Sitzungsberichte der Akademie der Wissenschaften in Wien, Mathematisch-Naturwissenschaftliche Klasse, Abteilung IIa, 136, 271–306, 1927.

Krauss, K. W., Cahoon, D. R., Allen, J. A., Ewel, K. C., Lynch, J. C., and Cormier, N.: Surface Elevation Change and Susceptibility of Different Mangrove Zones to Sea-Level Rise on Pacific High Islands of Micronesia, Ecosystems, 13, 129–143, https://doi.org/10.1007/s10021-009-9307-8, 2010.

Kumbier, K., Hughes, M. G., Rogers, K., and Woodroffe, C. D.: Inundation characteristics of mangrove and saltmarsh in micro-tidal estuaries, Estuarine, Coastal and Shelf Science, 261, 107 553, https://doi.org/10.1016/j.ecss.2021.107553, 2021a.

Kumbier, K., Hughes, M. G., Rogers, K., and Woodroffe, C. D.: Inundation characteristics of mangrove and saltmarsh in micro-tidal estuaries, Estuarine, Coastal and Shelf Science, 261, 107 553, https://doi.org/10.1016/j.ecss.2021.107553, 2021b.

Kumbier, K., Hughes, M. G., Carvalho, R. C., and Woodroffe, C. D.: Intertidal wetland geomorphology influences main channel hydrodynamics in a mature barrier estuary, Estuarine, Coastal and Shelf Science, 267, 107 783, https://doi.org/10.1016/j.ecss.2022.107783, 2022.

Lal, K. K., Woodroffe, C. D., Zawadzki, A., and Rogers, K.: Coastal wetland elevation dynamics, sedimentation, and accommodation space across timescales, Estuaries and Coasts, 47, 1828–1843, https://doi.org/10.1007/s12237-023-01308-5, 2024.

Lee, S. Y., Primavera, J. H., Dahdouh-Guebas, F., McKee, K., Bosire, J. O., Cannicci, S., Diele, K., Fromard, F., Koedam, N., Marchand, C., et al.: Ecological role and services of tropical mangrove ecosystems: a reassessment, Global ecology and biogeography, 23, 726–743, https://doi.org/10.1111/geb.12155, 2014.

Li, Z., Hodges, B. R., and Shen, X.: Modeling hypersalinity caused by evaporation and surface–subsurface exchange in a coastal marsh, Journal of Hydrology, 618, 129 268, https://doi.org/10.1016/j.jhydrol.2023.129268, 2023.

Lorrain-Soligon, L., Robin, F., Bertin, X., Jankovic, M., Rousseau, P., Lelong, V., and Brischoux, F.: Long-term trends of salinity in coastal wetlands: Effects of climate, extreme weather events, and sea water level, Environmental Research, 237, 116 937, https://doi.org/10.1016/j.envres.2023.116937, 2023.

Lovelock, C. E., Cahoon, D. R., Friess, D. A., Guntenspergen, G. R., Krauss, K. W., Reef, R., Rogers, K., Saunders, M. L., Sidik, F., Swales, A., et al.: The vulnerability of Indo-Pacific mangrove forests to sea-level rise, Nature, 526, 559–563, https://doi.org/10.1038/nature15538, 2015.

Lévesque, Y., Walter, J., Chesnaux, R., Dugas, S., and Noel, D.: Electrical resistivity of saturated and unsaturated sediments in northeastern Canada, Environmental Earth Sciences, 82, https://doi.org/10.1007/s12665-023-10998-w, 2023.

Macreadie, P. I., Costa, M. D. P., Atwood, T. B., Friess, D. A., Kelleway, J. J., Kennedy, H., Lovelock, C. E., Serrano, O., and Duarte, C. M.: Blue carbon as a natural climate solution, Nature Reviews Earth & Environment, 2, 826–839, https://doi.org/10.1038/s43017-021-00224-1, 2021.

Malone, B. and Searle, R.: Updating the Australian digital soil texture mapping (Part 1*): re-calibration of field soil texture class centroids and description of a field soil texture conversion algorithm, Soil Research, 59, 419–434, https://doi.org/10.1071/SR20283, 2021.

McDougall, T. J. and Barker, P. M.: Getting started with TEOS-10 and the Gibbs Seawater (GSW) Oceanographic Toolbox, 28pp., SCOR/IAPSO WG127, 2011.

https://doi.org/10.5194/egusphere-2026-1398
Preprint. Discussion started: 8 April 2026

MHL: NSW Tidal Planes Analysis 2001-2020, https://s3-ap-southeast-2.amazonaws.com/www-data.manly.hydraulics.works/www/publications/oeh/reports/MHL2786%20NSW%20tidal%20planes%20analysis%202001-2020%20final.pdf.

Owers, C. J., Rogers, K., Mazumder, D., and Woodroffe, C. D.: Spatial Variation in Carbon Storage: A Case Study for Currambene Creek, NSW, Australia, Journal of Coastal Research, 75, 1297–1301, https://doi.org/10.2112/SI75-260.1, 2016a.

Owers, C. J., Rogers, K., and Woodroffe, C. D.: Identifying spatial variability and complexity in wetland vegetation using an object-based approach, International Journal of Remote Sensing, 37, 4296–4316, https://doi.org/10.1080/01431161.2016.1211349, 2016b.

Owers, C. J., Woodroffe, C. D., Mazumder, D., and Rogers, K.: Carbon storage in coastal wetlands is related to elevation and how it changes over time, Estuarine, Coastal and Shelf Science, 267, 107 775, https://doi.org/10.1016/j.ecss.2022.107775, 2022.

Palombi, B., Power, H., Reinhard, P., Tunstill, K., Brown, W., Callen, A., and Rau, G.: Groundwater-Surface Water Interactions in Intermittently Closed and Open Lake and Lagoon (ICOLL) Wetlands: Implications for Salinity and Ecological Functioning, Ecohydrology, 19, https://doi.org/10.1002/eco.70149, 2026.

Pennings, S. C., Grant, M.-B., and Bertness, M. D.: Plant zonation in low-latitude salt marshes: disentangling the roles of flooding, salinity and competition, Journal of Ecology, 93, 159–167, https://doi.org/10.1111/j.1365-2745.2004.00959.x, : https://onlinelibrary.wiley.com/doi/pdf/10.1111/j.1365-2745.2004.00959.x, 2005.

Prihantono, J., Nakamura, T., Nadaoka, K., Solihuddin, T., Pryambodo, D. G., Ramdhan, M., Adi, N. S., Ilham, Wirasatriya, A., and Widada, S.: Seasonal groundwater salinity dynamics in the mangrove supratidal zones based on shallow groundwater salinity and electrical resistivity imaging data, Wetlands Ecology and Management, 31, 435–448, https://doi.org/10.1007/s11273-023-09926-3, 2023.

Rau, G. C., Post, V. E. A., Shanafield, M., Krekeler, T., Banks, E. W., and Blum, P.: Error in hydraulic head and gradient time-series measurements: a quantitative appraisal, Hydrology and Earth System Sciences, 23, 3603–3629, https://doi.org/10.5194/hess-23-3603-2019, 2019.

Redelstein, R., Dinter, T., Hertel, D., and Leuschner, C.: Effects of Inundation, Nutrient Availability and Plant Species Diversity on Fine Root Mass and Morphology Across a Saltmarsh Flooding Gradient, Frontiers in Plant Science, 9, https://doi.org/10.3389/fpls.2018.00098, 2018.

Rogers, K., Saintilan, N., and Woodroffe, C. D.: Surface elevation change and vegetation distribution dynamics in a subtropical coastal wetland: Implications for coastal wetland response to climate change, Estuarine, Coastal and Shelf Science, 149, 46–56, https://doi.org/10.1016/j.ecss.2014.07.009, 2014.

Rogers, K., Kelleway, J. J., Saintilan, N., Megonigal, J. P., Adams, J. B., Holmquist, J. R., Lu, M., Schile-Beers, L., Zawadzki, A., Mazumder, D., et al.: Wetland carbon storage controlled by millennial-scale variation in relative sea-level rise, Nature, 567, 91–95, https://doi.org/10.1038/s41586-019-0951-7, 2019.

Rogers, K., Zawadzki, A., Mogensen, L. A., and Saintilan, N.: Coastal wetland surface elevation change is dynamically related to accommodation space and influenced by sedimentation and sea-level rise over decadal timescales, Frontiers in Marine Science, 9, 807 588, https://doi.org/10.3389/fmars.2022.807588, 2022.

Rosas, J., Lopez, O., Missimer, T. M., Coulibaly, K. M., Dehwah, A. H., Sesler, K., Lujan, L. R., and Mantilla, D.: Determination of Hydraulic Conductivity from Grain-Size Distribution for Different Depositional Environments, Groundwater, 52, 399–413, https://doi.org/10.1111/gwat.12078, 2013.

Roy, P. S., Williams, R. J., Jones, A. R., Yassini, I., Gibbs, P. J., Coates, B., West, R. J., Scanes, P. R., Hudson, J. P., and Nichol, S.: Structure and Function of South-east Australian Estuaries, Estuarine, Coastal and Shelf Science, 53, 351–384, https://doi.org/10.1006/ecss.2001.0796, 2001.

https://doi.org/10.5194/egusphere-2026-1398
Preprint. Discussion started: 8 April 2026

Sadat-Noori, M., Andersen, M. S., Rutlidge, H., and Glamore, W.: Coastal Wetland Restoration Effects on Carbon Dynamics: A Groundwater Perspective, Reviews of Geophysics, 63, e2025RG000 895, https://doi.org/https://doi.org/10.1029/2025RG000895, e2025RG000895 2025RG000895, 2025.

Saenger, P.: Mangrove ecology, silviculture and conservation, Springer Science & Business Media, 2002.

Saintilan, N.: Biogeography of Australian saltmarsh plants, vol. 34 of *Australian Saltmarsh Ecology*, 2009.

Saintilan, N., Rogers, K., Kelleway, J. J., Ens, E., and Sloane, D. R.: Climate Change Impacts on the Coastal Wetlands of Australia, Wetlands, 39, 1145–1154, https://doi.org/10.1007/s13157-018-1016-7, 2019.

Saintilan, N., Horton, B., Törnqvist, T. E., Ashe, E. L., Khan, N. S., Schuerch, M., Perry, C., Kopp, R. E., Garner, G. G., Murray, N., et al.: Widespread retreat of coastal habitat is likely at warming levels above 1.5 C, Nature, 621, 112–119, https://doi.org/10.1038/s41586-023-06448-z, 2023a.

Saintilan, N., Sun, Y., Lovelock, C. E., Rogers, K., Goddard, M., Hutley, L. B., Kelleway, J., Mosley, L., Dittmann, S., Cormier, N., Lal, K. K., and Jones, A.: Vertical accretion trends in Australian tidal wetlands, Estuaries and Coasts, https://doi.org/10.1007/s12237-023-01267-x, 2023b.

Shen, C., Zhang, C., Xin, P., Kong, J., and Li, L.: Salt Dynamics in Coastal Marshes: Formation of Hypersaline Zones, Water Resources Research, 54, 3259–3276, https://doi.org/10.1029/2017wr022021, 2018.

Sherif, M. M. and Singh, V. P.: Saltwater Intrusion, p. 269–316, Springer Netherlands, ISBN 9789401586801, https://doi.org/10.1007/978-94-015-8680-1_10, 1996.

Thom, B. G.: Mangrove ecology and deltaic geomorphology: Tabasco, Mexico, The Journal of Ecology, pp. 301–343, https://doi.org/10.2307/2257879, 1967.

Townend, I., Fletcher, C., Knappen, M., and Rossington, K.: A review of salt marsh dynamics, Water and Environment Journal, 25, 477–488, https://doi.org/10.1111/j.1747-6593.2010.00243.x, 2011.

Tran, D. B., Hoang, T. V., and Dargusch, P.: An assessment of the carbon stocks and sodicity tolerance of disturbed Melaleuca forests in Southern Vietnam, Carbon Balance and Management, 10, 15, https://doi.org/10.1186/s13021-015-0025-6, 2015.

Victoria, A.: Coast Sword-sedge, https://vro.agriculture.vic.gov.au/dpi/vro/vrosite.nsf/pages/sipsaltcoastswordsedge, 2020.

Vienken, T. and Dietrich, P.: Discussion of papers: determination of hydraulic conductivity from grain-size distribution for different depositional environments, Ground Water, 52, 823–824, 2014.

Woodroffe, C. D., Rogers, K., McKee, K. L., Lovelock, C. E., Mendelssohn, I., and Saintilan, N.: Mangrove sedimentation and response to relative sea-level rise, Annual review of marine science, 8, 243–266, https://doi.org/10.1146/annurev-marine-122414-034025, 2016.

Wriedt, T.: Mie theory: a review, The Mie theory: Basics and applications, pp. 53–71, https://doi.org/10.1007/978-3-642-28738-12, 2012.

Zhang, H.: Anisotrope Variation der gesättigten Wasserleitfähigkeit einer unterschiedlich beweideten Salzmarsch im Deichvorland, Zeitschrift für Pflanzenernährung und Bodenkunde, 159, 129–135, https://doi.org/10.1002/jpln.1996.3581590205, 1996.

Zhang, Y., Li, W., Sun, G., Miao, G., Noormets, A., Emanuel, R., and King, J. S.: Understanding coastal wetland hydrology with a new regional-scale, process-based hydrological model, Hydrological Processes, 32, 3158–3173, https://doi.org/10.1002/hyp.13247, 2018.